IPP-Report

Max-Planck-Institut
für Plasmaphysik

Martin Balden

Assessment of the Si content of Si impregnated Carbon-Carbon Fibre composite

IPP 17/2
October 2004

Assessment of the Si content of Si impregnated Carbon-Carbon Fibre composite

EFDA Ref: TW3-TVM-CFCQ1

M. Balden

Max-Planck-Institut für Plasmaphysik, EURATOM Association, D-85748 Garching, Germany

Garching, October 2004

Assessment of the Si content of Si impregnated Carbon-Carbon Fibre composite

EFDA Ref: TW3-TVM-CFCQ1

M. Balden

Max-Planck-Institut für Plasmaphysik, EURATOM Association, D-85748 Garching, Germany

Abstract

The content, distribution and chemical state of silicon in the material NS31 of the delivery 2004 were investigated by MeV ion beam analysis, scanning electron microscopy and X-ray diffraction. An average Si concentration of 4-5 at.% (9-11 wt.%) is found. The material is inhomogeneously doped on the length scale of 1 mm. A dependence of the Si concentration on the position in the original block is not detectable. The Si is partly free elemental silicon and partly silicon carbide. A small amount of the Si in the surface is oxidised (<2 at.% O). The material is not thermally stable for temperatures above 1470 K.

Table of Content

1. Introduction

In the ITER divertor, a variety of materials for the plasma facing surfaces of the high heat flux components will be used. The favoured material at the present time is a Carbon-Carbon fibre composite (CFC) with good thermal conductivity and good mechanical stability (NB31, SEPCARB, SNECMA, France). In addition to pure CFC tiles, CFC doped with 8±2 at.% silicon may be used (NS31, SEPCARB, SNECMA, France).

Because of the importance of the correct silicon level for reaching the optimal oxidation resistance, the silicon content of the material was the main subject of this investigation. The silicon distribution and its chemical form within the samples were also studied. Additionally, the thermal stability of the material was checked. The performed investigations are analogous to a previous study initiated by NET, see Appendix **A**.

2. Experimental

2.1. Specimens

Seven specimens were provided directly from EFDA in March 2004. They are originated from two pieces of NS31 (Block No. **3** and **33**). More detailed information about the delivery of the blocks is given in Appendix **B**. The position of the specimens within the blocks can be seen from the cutting plans in Appendix **B**. All specimens are plates with a length of 50 or 65 mm, a width of 5 or 12 mm, and a thickness of 1 mm. No cleaning procedure was applied to the specimens; they were investigated as delivered. One of the specimens (**B2d**) was further cut with an impact knife edge in five specimen of ~13 mm length for the thermal stability tests.

2.2. Determination of the Si content and its distribution by ion beam analysis (IBA)

Backscattering spectrometry of 2.0 MeV ^{4}He ions and 1.5 MeV protons was used to obtain the Si content, the depth distribution near to the surface and the lateral distribution of the Si in the specimens. The ion beam hit the target at normal incidence. The scattering angle was 165°. Ion fluences between 5 μC and 10 μC were accumulated for each spectrum.

To study the lateral Si distribution the specimens were analysed along their length direction on lines (line scans). Usually, each analysing position was separated 1 mm from the next one, while the size of the analysing spot was 1x1 mm^2. For some specimens with 12 mm width, line scans were measured 4 mm left or right of the usual central line.

The silicon concentration c_{Si} is evaluated by using the program SIMNRA [1]. The intensity of backscattered ^{4}He and protons at the backscattering energy of 830 keV and 1200 keV, respectively, were used to obtain values of Si concentration for each analysing position. These energies correspond to depths of about 0.6 and 1.5 μm, respectively. For more

details about information depth and conversion of intensity to Si concentration are given in Appendix **C**. The silicon concentration is always given in atomic percent.

All spectra of each specimen are summed up to obtain the average Si concentration of the specimen with good statistics. The total investigated area per specimen varies between 30 and 150 mm^2. To achieve one value for the Si concentration representative for the material NS31 of the delivery 2004, all measured spectra were averaged for both analysing ion types. (More details about the averaging can be found in Appendix **D**).

2.3. Determination of the chemical state of the Si by X-ray diffraction (XRD) and scanning electron microscopy (SEM)

The crystal phase and therefore the chemical state of the Si were determined with the X-ray diffraction using normal Θ-2Θ scans in parallel beam configuration. Elemental silicon is distinguishable from silicon carbide (SiC) by the presence of its diffraction peaks.

In principal, the amount of both phase can be determined, if the specimen consist of a perfect powder and reference diffraction pattern exist [2]. But the specimens do not fulfil the requirement of perfect powder. Therefore, the amount of both phases could not be determined.

Because the X-ray beam was collimated to a circular beam with 2 mm diameter, the analysed area was restricted. But due to the experimental geometry, the resulting spot on the specimen is elliptic. Its elongation decreases with increasing scattering angle (2Θ), i.e. in a typical diffraction spectrum from 20° to 120° it varied from 11 to 2.3 mm, respectively. More details to the spot size and the XRD pattern of Si and SiC are given in Appendix **E**.

The presence of elemental Si beside SiC and graphite can be visualised by back scattered electrons in SEM with its typical high lateral resolution (<<1 µm). The mean atomic number for Si is higher than for SiC and therefore regions with elemental Si appear brighter in the images. Beyond that, the chemical composition of the surface was measured by energy dispersive X-ray spectrometry (EDX).

2.4. Heat treatment

Smaller pieces of one specimen (**B2d**) were used for the thermal stability tests. The mass of the pieces before and after (0.3-0.4 g) the heat treatment were measured. The pieces were put into a graphite crucible and the heating was performed by induction inside a glass tube at a pressure of ~10^{-4} Pa.

The temperature of the crucible was measured by an IR-pyrometer (0.4-1.1 µm) and an incandescence pyrometer. Both pyrometers comparing only light intensity coming from the crucible. The effective emissivity of 80% was used. Due to the uncertainty of the effective

emissivity (which may be changed during test) and due to an insufficient power control of the induction generator, the accuracy of the temperature setting is not better than ±50 K.

In order to know the mass loss by water or other desorbing species at low temperatures, one specimen was heated for 1 hour at ~700 K. The weight loss was 0.06 mg, which is assumed to be the same for all specimens.

Heating experiments were carried out at three different temperatures (1470, 1570 and 1700 K) with 10 minutes holding time. The specimen heated at 1470 K was further heated for 60 minutes, i.e. altogether 70 minutes. The composition and the chemical state were investigated between the two heat treatments.

2.5. Used equipment

For the ion beam analysis, the 3-MeV-tandem accelerator (High Voltage) and the surface analysis chamber (RKS) of the Material Research division were used. The X-ray diffraction measurements were performed with the X-ray diffractometer (XRD-3003 PTS, Seifert). Images of the surface were obtained with a scanning electron microscope (XL30 ESEM, Philips) with X-ray spectrometer (Phoenix, EDAX).

For the thermal stability test a micro balance (MC21S, Sartorius), a glass tube with vacuum pump station and the induction generator (F&H), an incandescence pyrometer (Mikro-Pyrometer, Pyro-Werk GmbH), and an IR-pyrometer (Infratherm IS-8, Impac Electronic GmbH) were used. The set-up for the heating is shown in Appendix **F**.

3. Results

3.1. Silicon content and distribution

Figures **1** and **2** summarise the averaged backscattering spectra for all specimen and line scans. By comparing with simulated spectra of homogeneously Si-doped graphite and the averaged spectrum for the delivery 1996, it results that the Si content of delivery 2004 is about 4-5 at.%. Therefore, the Si concentration is less than in the earlier delivery and less than specified (8±2 at.%).

The presence of heavier impurities is neglected for the determination of the Si concentration (see section **3.2.**), i.e. no background subtraction was made. The systematic error introduced by the lack of a background correction increases the Si concentration in average by maximal +0.5 at.%, i.e. the average Si concentration would be closer to 4 than 5 at.%.

In figure **3** the lateral variation of the Si content for an area of 1 mm^2, which is between 0 and 30 at.% Si, is illustrated by the vertical spread. (Similar data for NS31 of delivery 1996 are given in Appendix **G**.) The strong inhomogeneity of the Si concentration in the material yields to slight differences in the Si concentration determined with ^{4}He ions and protons mainly, because the accuracy of beam positioning for the same line scan is not better than 0.1 mm. By comparing the averaged Si concentration per line scan and the variation between the specimens (Tab. **1**), it can not be concluded whether the Si concentration exhibits a change with the specimen position in the NS31 block or not (Appendix **B**). Also, no significant increase or decrease of the Si concentration at the ends of the line scans on the specimens is observed (Appendix **G**). Therefore, a dependence of the Si concentration on the position in the original block is not detectable.

The depth distribution of the Si is quite homogeneous in the information depth of ~10 µm of the ion beam analysis (Figs. **1a** and **2a**).

Figure **4** shows nine combined SEM images with low magnification. The lateral inhomogeneity on the 1 mm scale is clearly visible in this overview.

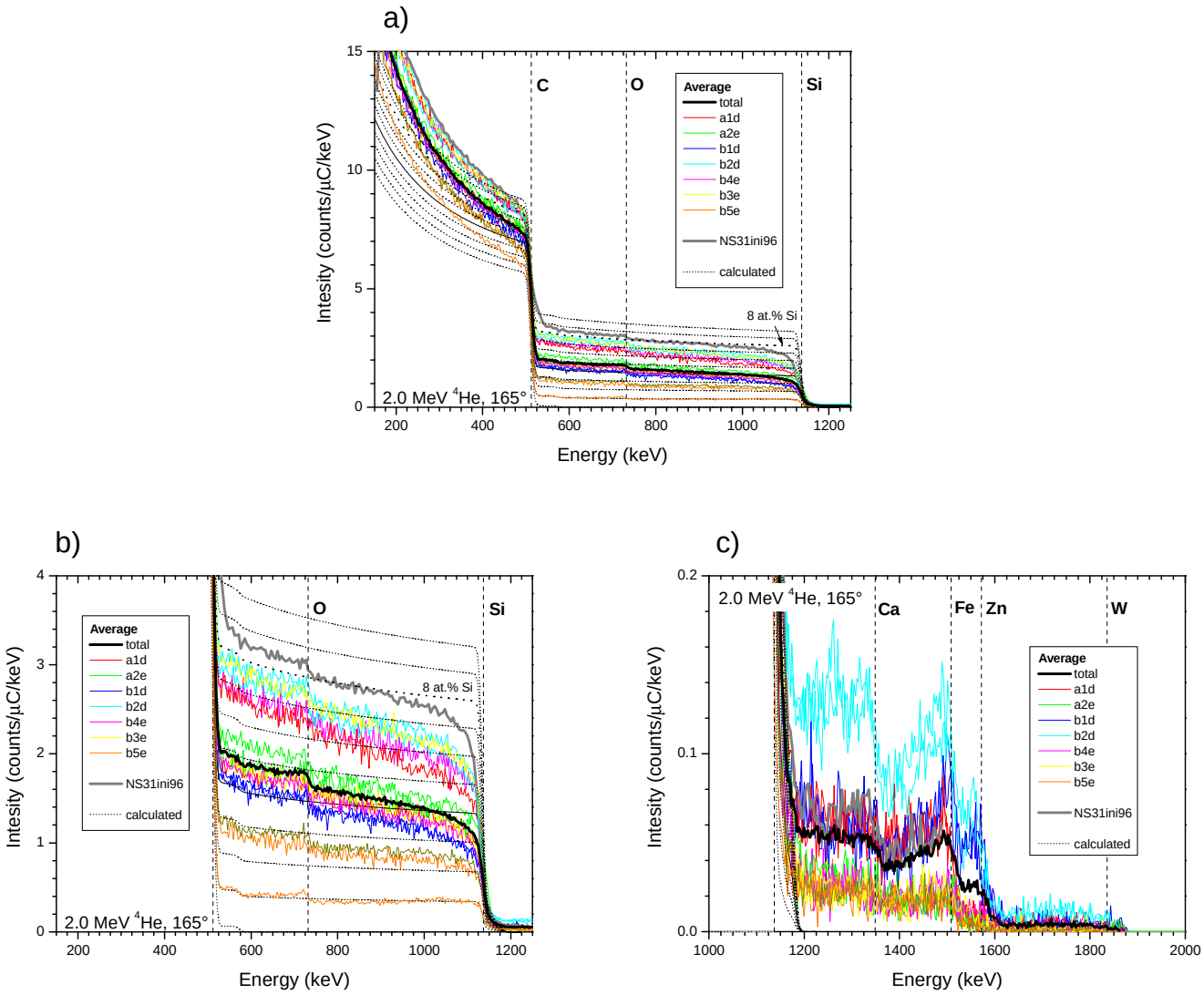

***FIGURE 1**: Averaged spectra of all seven specimens obtained by 2.0 MeV ^{4}Helium backscattering: a) complete spectra, b) and c) blow-ups. Different line scans along the same specimen are represented by different line thickness. Simulated spectra for homogeneously Si-doped graphite are shown (dotted lines). The Si concentration of the calculated spectra vary stepwise by 1 at.% Si. The maximal backscattering energy for some elements (edges) are exhibited by vertical lines. For comparison the averaged spectrum for the delivery 1996 is inserted (Appendix **A**).*

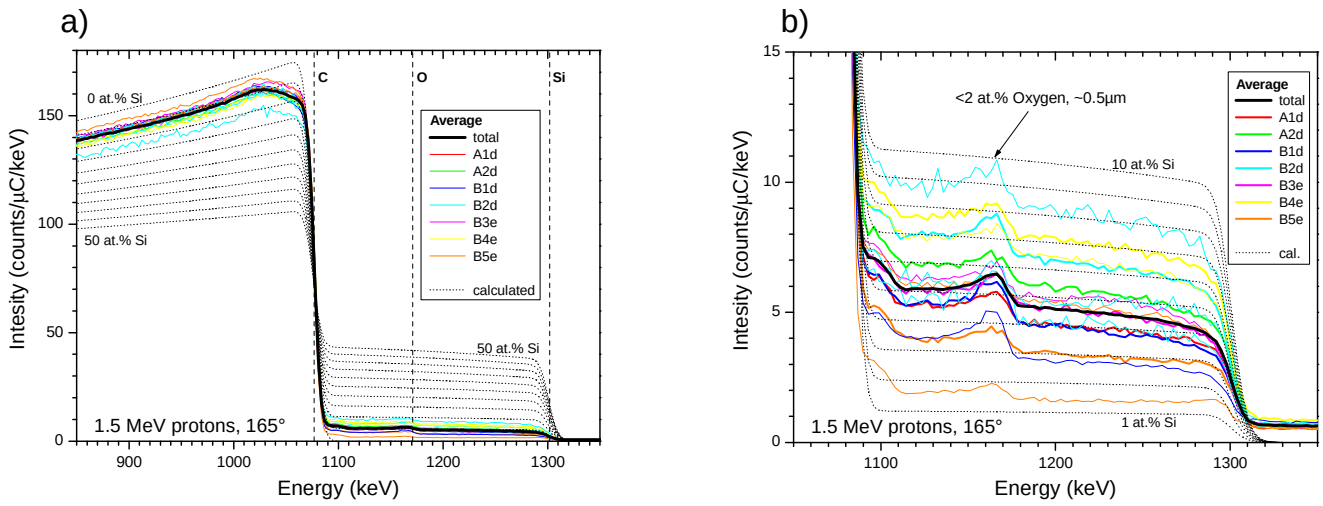

***FIGURE 2**: Averaged spectra of all seven specimens obtained by 1.5 MeV proton backscattering: a) complete spectra and b) blow-up. Different line scans along the same specimen are represented by different line thickness. Simulated spectra for homogeneously Si-doped graphite are shown (dotted lines). The Si concentration of the calculated spectra varies in a) and b) stepwise by 5 and 1 at.% Si, respectively. The maximal backscattering energy for some elements (edges) are exhibited by vertical lines.*

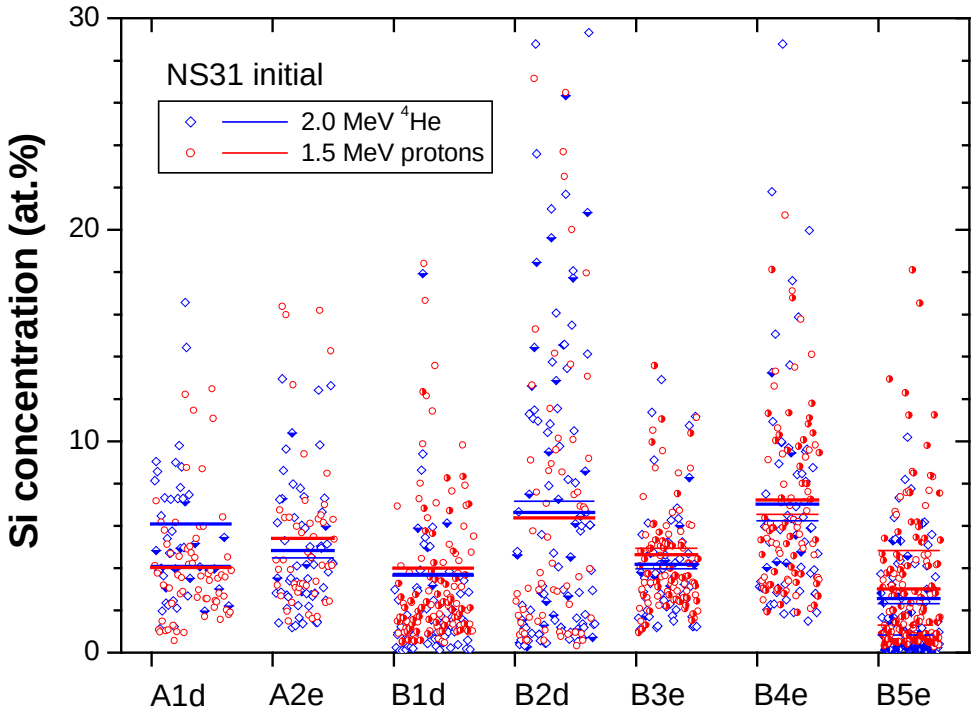

***FIGURE 3**: Si concentration for each single spectrum measured on the seven specimens and used for the averaged spectra (Figs. **1** and **2**). The different line scans on each specimen are indicated by different fillings of the symbols. The average value per line scan is shown as horizontal bars. Each data point represents the average concentration of an area of ~1 mm^2. The spread in x direction of the data represents the position along the specimen.*

***TABLE 1**: Average Si concentrations for all scans on the seven initial NS31 specimen. The numbers in italic are Si concentrations for the line scans left or right of the central line scan (larger numbers).*

Specimen	2.0 MeV ^{4}He [at.% Si]			1.5 MeV protons [at.% Si]		
A1d	6.09	*4.12*		4.03		
A2e	4.84	*4.48*		5.41		
B1d	3.68	*3.75*		4.00		
B2d	6.64	*7.16*		6.38		
B3e	4.18	*3.97*		4.64	*4.94*	
B4e	7.02	*6.24*		7.22	*6.55*	
B5e	2.57	*2.32*	*0.83*	3.02	*4.84*	*1.31*

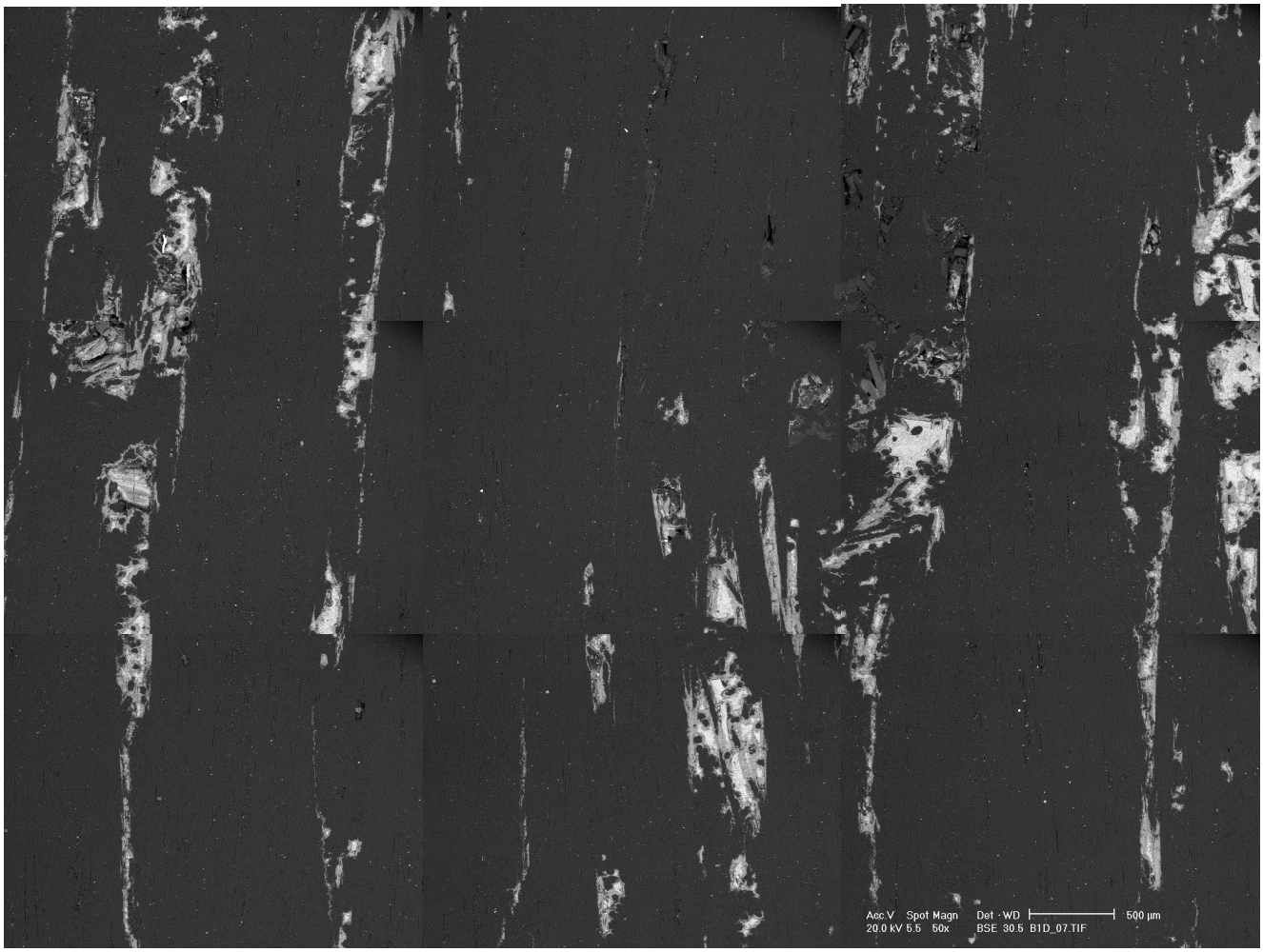

***FIGURE 4**: Nine SEM images of backscattered electrons in low magnification of specimen **B1d** are merged together to cover an area of ~7.3×5.4 mm^2. (Another example of overview is given in Appendix **G**.)*

3.2. Chemical state of the silicon

Three phases are detected with X-ray diffraction (XRD): graphite, silicon carbide, and elemental silicon (Fig. **5**). Unfortunately, the quantification of the ratio elemental Si to Si bonded as SiC is not possible. SEM images (Fig. **6a**) and associated EDX studies (Figs. **6b-d**) support that a large fraction of the detected silicon is elemental.

Small quantities of oxygen are observed with EDX (Fig. **6b**). This oxygen is mostly bonded in the first 0.5 µm as IBA spectra are indicating (Figs. **1b** and **2b**). Its average concentration is below 2 at.%.

Additional, some other impurities are detected with IBA (Fig. **1c**). The determination of impurity elements and concentrations is not easy definable. It might be Ca, Fe, Zn, and W with average concentration of less than 0.03, 0.03, 0.015, and 0.001 at.%, respectively.

Calcium, iron, and tungsten were also observed in SEM. Calcium is typically found as particles of $CaCO_3$ on top of the material. Tungsten or WC show up as very small particles (<1 µm). Some particle of iron were observed, which may be introduced by the cutting process. But in one case the Fe is imbedded in the silicon, indicating that the specimen must be heated fare above 1000 K after the introduction of the iron (Fig. **H2** in Appendix **H**). These impurities might be introduced by the preparation procedure (see section **3.3.**).

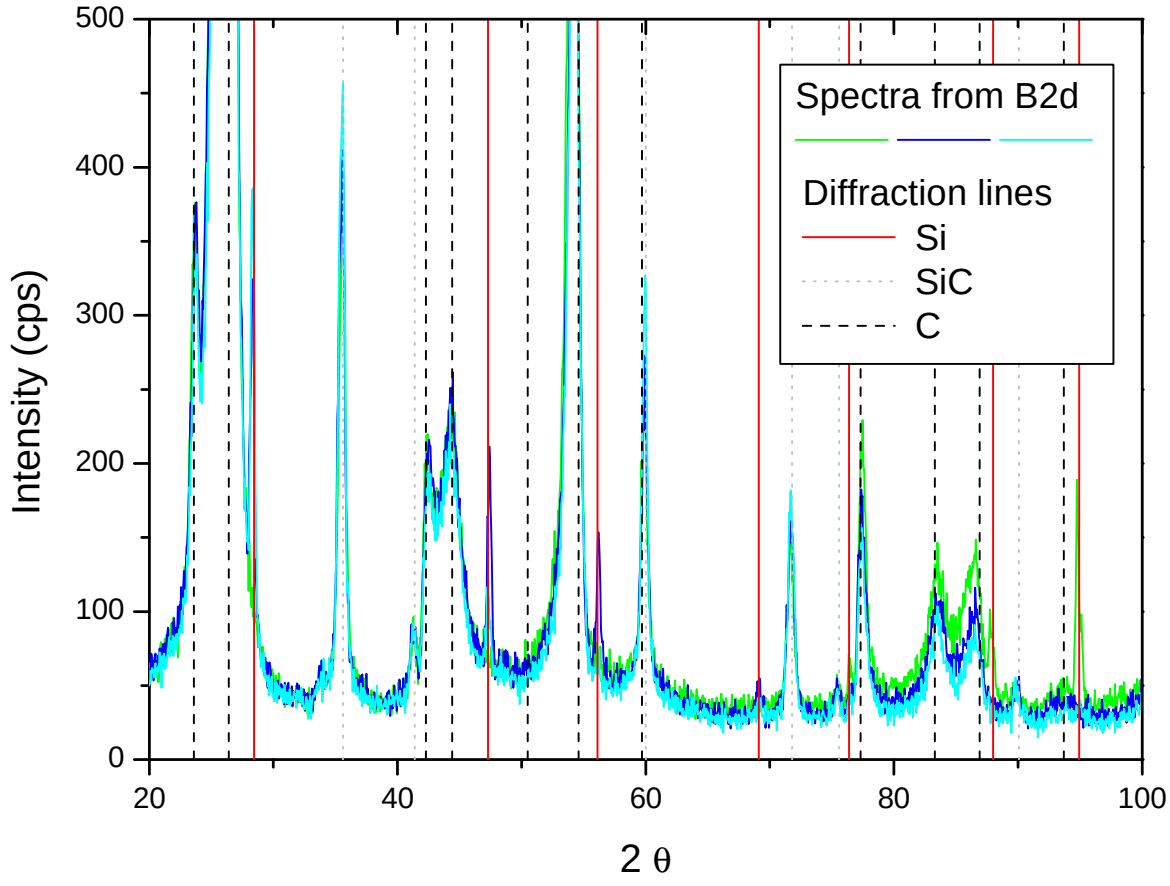

***FIGURE 5**: XRD spectra of three positions on the initial **B2d**. Positions of diffraction peaks for C, Si, and SiC are marked by vertical lines. Elemental Si is visible, but not always all diffraction peaks are present.*

a)

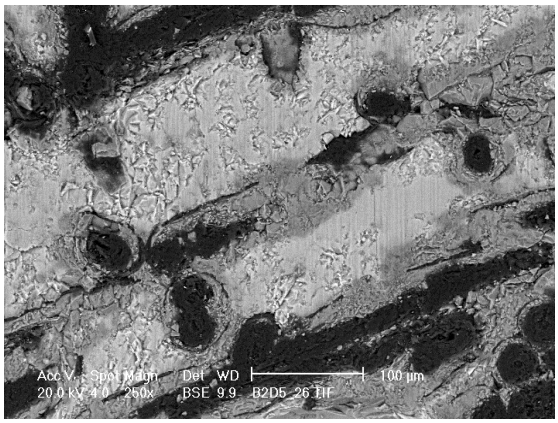

b)

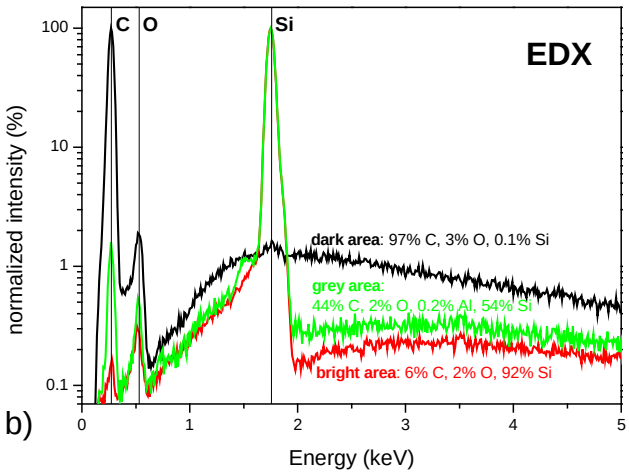

c)

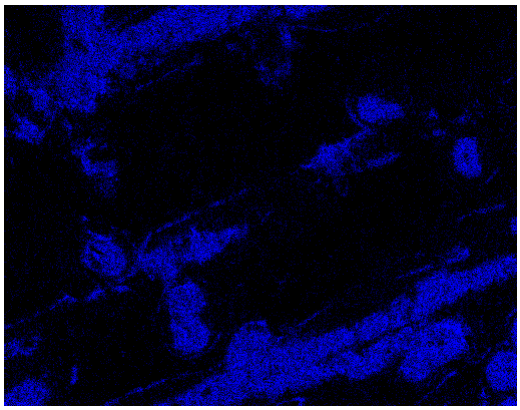

d)

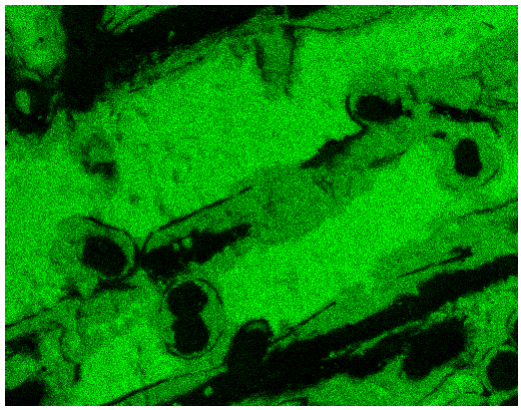

***FIGURE 6**: a) SEM image of backscattered electrons of the initial specimen **B2d #5**. Dark, grey, and bright areas represent graphite, elemental silicon, and silicon carbide, respectively; b) EDX spectra from such dark, grey and bright areas with a rough quantification; c) EDX mapping for the C_K light; d) EDX mapping for the Si_K light.*

3.3. Thermal stability

The weight loss resulting from the four heating tests are compiled in table **2**. These results clearly demonstrate that the material is not thermal stable for temperatures above 1470 K.

The IBA results for the heated specimen are summarised in the figures **7** to **9**. An increase of the Si concentration on the surface is clearly indicated by heating above 1500 K. The increase raises further close to the surface (< 1 µm), which is signified by the different average values in figure **9** for the two analysing ion species with their different information depth (~0.6 and ~1.5 µm) and by the increase in the signal corresponding to Si (Fig. **7**, >1100 keV). Additionally, a depletion of Si in the outermost surface layer is observed for the highest temperature (1700 K) demonstrated by the increase in the signal corresponding to the C just below the surface (Fig. **7**, 1060-1080 keV; Fig. **8**, 450-510 keV) and by the off set of the signal corresponding to Si (Fig. **7**, <1300 keV; Fig. **8**, ~1100 keV).

For the lowest heating temperature (1470 K) significant changes are not evident from the IBA measurements. But in SEM images changes are clearly observed (Fig. **10**). The Si wetted surface area increases with the heating. The area covered with elemental Si decreases.

Areas with elemental Si were not observed anymore for the specimen heated above 1500 K with SEM. Nevertheless, the free Si is not all reacted to SiC or evaporated from the specimen as peaks of elemental Si in XRD spectra of these specimens indicate. The appearance of Si peaks is reduced on the specimen **B2d #4** and #**5**, but for some investigated positions definitely Si peaks exist, i.e. free Si.

The impurity content of the surface is reduced by the heating (Fig. **8**). It is unclear if the impurities evaporate or if they diffuse into the material. If the latter is right, it is reasonable that the observed impurities are introduced by the preparation treatment and are only located at the surface, i.e. that they have no influence on the obtained Si concentration in section **3.1**.

TABLE 2*: Weight losses due to heating tests at various temperatures and holding times are given. For obtaining the absolute and relative weight losses, the desorption of gases at lower temperatures is taken into account (0.06 mg).*

Specimen	Temperature	Total holding time	Abs. weight loss	Rel. weight loss
B2D #3	1470 K	10 min.	0.10 mg	0.03 %
B2D #3	1470 K	70 min.	0.48 mg	0.14 %
B2D #4	1570 K	10 min.	1.04 mg	0.32 %
B2D #5	1700 K	10 min.	2.77 mg	0.81 %

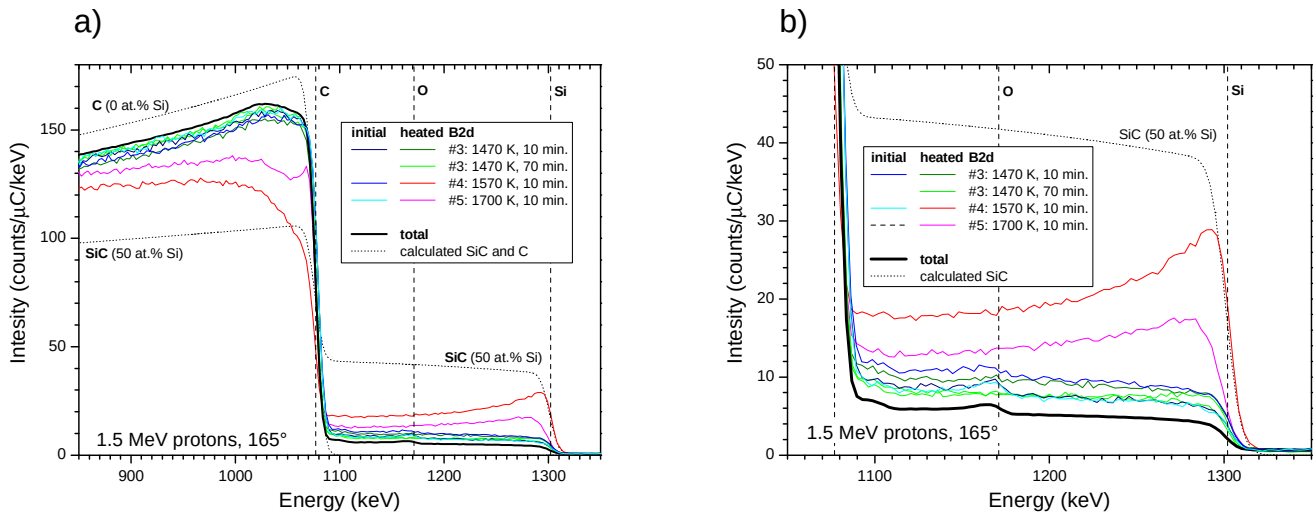

***FIGURE 7**: Averaged spectra of the specimen before (initial) and after the heat treatment obtained by 1.5 MeV proton backscattering: a) complete spectra and b) blow-up. Different lines scans along the same specimen are represented by different line thickness. Simulated spectra for SiC and C are shown (dotted lines). The maximal backscattering energy for some elements (edges) are exhibited by vertical lines. For comparison the averaged spectrum of the delivery 2004 is inserted. (Fig. **2**).*

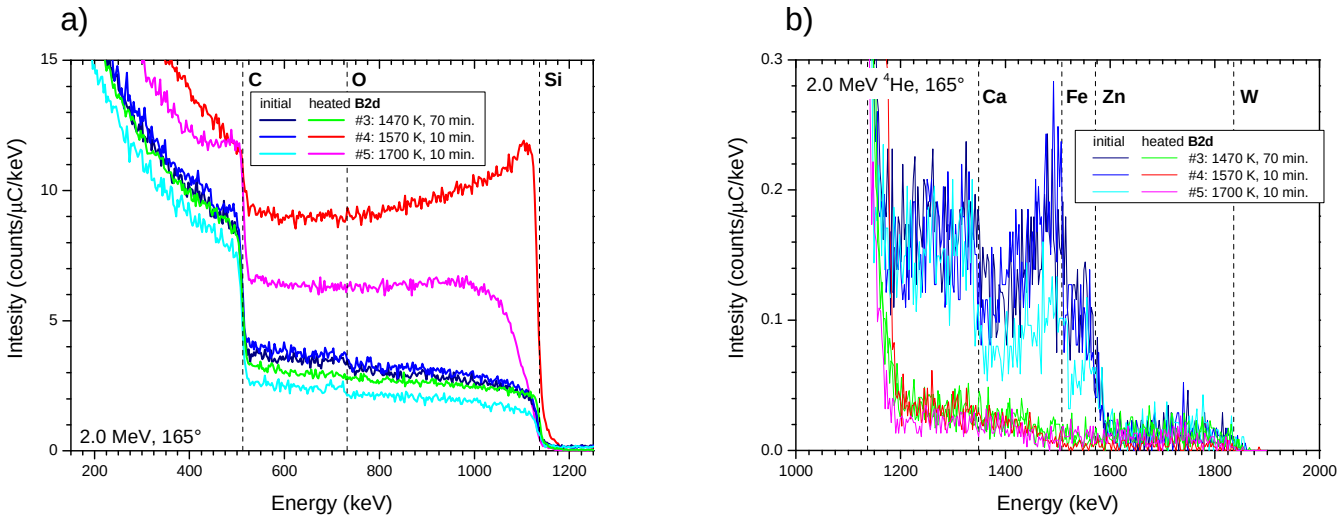

***FIGURE 8**: Averaged spectra of the specimen before (initial) and after the heat treatment obtained by 2.0 MeV ^{4}Helium backscattering: a) complete spectra and b) blow-up to visualize the impurity content. The maximal backscattering energy for some elements (edges) are exhibited by vertical lines.*

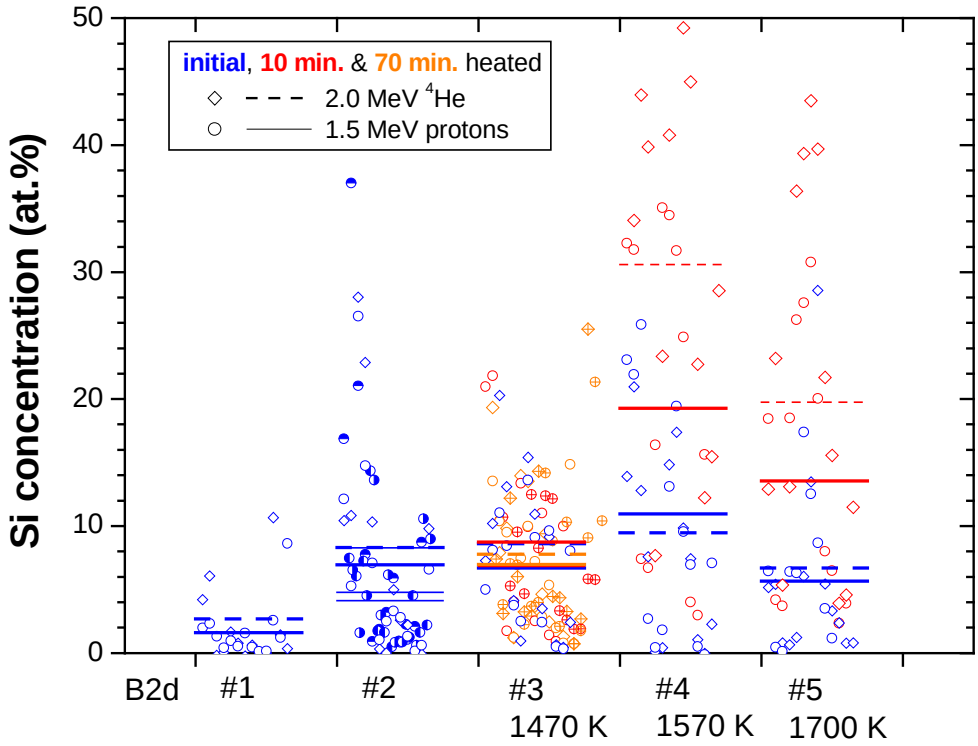

***FIGURE 9**: Si concentration for each single spectrum measured on the five specimen pieces of **B2d** before and after the heat treatments (colours) obtained by 2.0 MeV ^{4}Helium and 1.5 MeV proton backscattering. The different line scans on each specimen are indicated by different fillings of the symbols. The average value per line scan is shown as horizontal bars. Each data point represents the average concentration of an area of ~1 mm^2. The spread in x direction of the data represents the position along the specimen.*

a)

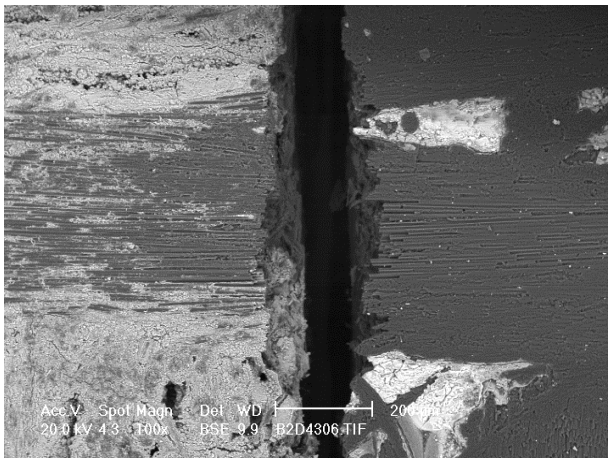

b)

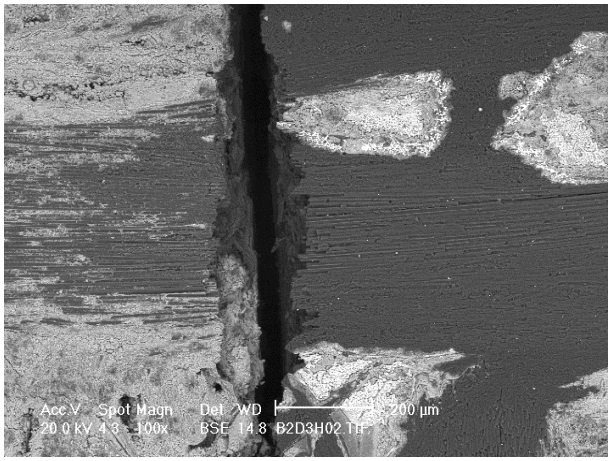

c)

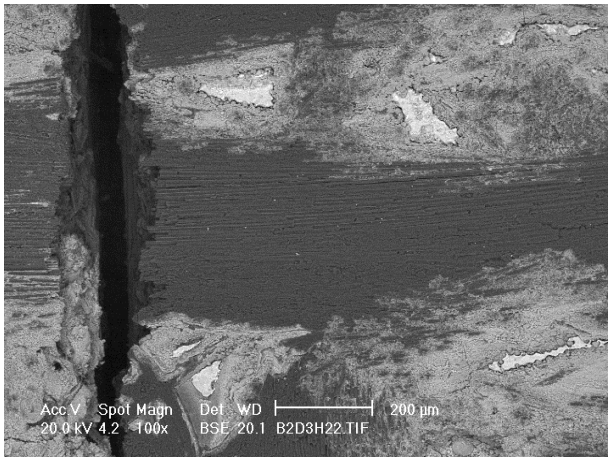

***FIGURE 10**: SEM images of backscattered electrons. The specimens **B2d #4** after heating for 10 minutes at 1570 K is shown on the left in all three images. The specimen B2d #3 is presented on the right in the three images, a) initial, b) after heating for 10 minutes and c) for 70 minutes at 1470 K. The area covered with SiC (grey areas) increases with heating, while the amount of elemental Si decreases.*

4. Summary

The content, distribution and chemical state of silicon in the material NS31 of the delivery 2004 were investigated by MeV ion beam analysis, scanning electron microscopy and X-ray diffraction.

The average Si concentration for the NS31 of delivery 2004 is only 4-5 at.% (9-11 wt.%), i.e. less than the specified 8±2 at.% Si. This fibre composite material is inherently inhomogeneous on the length scale of 1 mm and therefore also the distribution of the Si. A dependence of the Si concentration on the position in the original block is not detectable, i.e. the Si concentration is not higher or lower on the surface of the blocks than in the bulk.

The Si is partly free elemental silicon and partly silicon carbide. This free Si is not thermally stable for temperatures above 1470 K.

Appendixes

Appendix A: Copy of the final report of NET contract ERB 5004 CT 97 0093 (NET / 97-457)

Final Report of NET Contract
ERB 5004 CT 97 0093 (NET / 97-457)

" Post-Test Examination of Divertor Mock-Up Tiles after High Power Load Testing "

M. Balden and J. Roth

Garching, 1. February 1999

1 Introduction

The disadvantages of carbon materials as plasma facing components are the chemical reactivity with hydrogen and oxygen and the large amount of retained tritium. The chemical reactivity could be reduced by dopants, e.g. silicon, boron, or titanium [1–14]. The distribution of the dopant in the surface zone affects the erosion behaviour of the material. For the tritium retention three different aspects are important: the trapped tritium in the implantation zone, the migration of tritium into the bulk of the plasma facing materials, and, in particular, co-deposition of tritium in the re-deposited material. All three aspects are affected in a different way by the dopants and by the microstructure of the material.

Normally, the thermal conductivity – necessary for handling the high power loads of transient events – is related to the microstructure of the materials and the perfection of the crystal structure. So, in graphitic materials a dopant reduces the thermal conductivity. However, in cooperation of Societe Europeenne de Propulsion (SEP), France, and NET Team, a silicon doped carbon fibre composite (CFC) has been developed with an optimized thermal conductivity [15]. This 3D CFC material, called NS31, has been now recommended as the ITER reference material (IDoMS Nr. G17 MI 22 97-05-21 F1) and is specified with the properties listed in table 1 and 2.

	Thermal diffusivity (10^{-6} m^2/s)			thermal conductivity (W/m K)		
	X	Y	Z	X	Y	Z
RT	200	66	60	304	100	91
1100 K	43	16	14	149	55	48
1300 K	39	15	12	141	54	43

TABLE 1: Thermal diffusivity and conductivity of NS31 as specified by SEP [15].

density	2.0 g/cm^3
silicon concentration	8–10 at. %
porosity	5 %
mean atomic mass	13.3–13.6 u
atomic density	0.9×10^{29} $at./m^3$

TABLE 2: Physical properties of NS31 as specified by SEP [15].

Usually, the evaporation of dopants is expected at elevated temperatures. This evaporation may influence the microstructure of the material and the dopant concentration near the surface (and perhaps of the bulk). Therefore, it may influence the erosion yield by ion bombardment and the tritium retention in the implantation zone, bulk, and co-deposited layers.

In this report the dopant distribution of initial ('as received') NS31 (delivery A, 1996) and the possible Si depletion at elevated temperature due to a heat treatment (1800 K for 2 hours) has been investigated. The erosion yield due to bombardment with deuterium of initial and heated NS31 and the deuterium content in the bombarded NS31 as well as in the re-deposited material has been determined. Also, the dopant distribution at the surface of a mock-up tile after thermal shock tests and of the initial material of two further deliveries (B, 1997 and C, 1998) has been measured.

2 Experimental Details

2.1 Samples and treatments

The material NS31 was places at our disposal by the NET Team as blocks from the deliveries A (1996), B (1997) and C (1998) from SEP and as a part of a mock-up tile after thermal shock tests machined from the material of the delivery A.

The blocks of NS31 were mechanically cut into small plates (usually $12\times15\times1$ mm^3) with respect to the three different values of thermal conductivity (X, Y, Z) and cleaned in an ultrasonic bath.

Some of the initial samples from the block of delivery A were heated in vacuum at 1800 K for 2 hours. For the heat treatment an induction oven was used and the temperature was controlled by an incandescence pyrometer. In order to obtain information on the bulk of heated NS31 (1 mm beneath the surface), some of the heated samples were cut once more. These faces are called 'cut' faces in the report.

Another set of samples was obtained by cutting the mock-up tile, which was exposed to 18 MW/m^2 power load for 1000 pulses of about 10 seconds in the 200 kW FE200 at Framatome in LeCreusot, France [16]. During the loading the material reaches a temperature above 2300 K.

In order to investigate the co-deposition of deuterium with the eroded material from a sample of delivery A, the eroded material was collected on special catcher plates (carbon substrate with a gold layer of about 800Å on top) during the erosion measurements with 3 keV D_3^+ ions. Only thin deposited layers with varying thickness across the catcher plates were created.

2.2 Scanning electron microscopy

In order to get a view of the surface topography scanning electron microscopy (SEM) was performed [17]. The information depth of the secondary electrons of the used 20 keV electron beam is about a few nm. Coupled with the topographic image from the secondary electrons the electron induced X-ray emission (EIXE) yields information on the composition of the material throughout the penetration depth of a electron beam of about 1–3 μm.

2.3 Backscattering spectrometry and nuclear reaction analysis

The silicon concentration and depth profile near the surface of NS31 was determined using backscattering spectrometry of 2.0 MeV ^{4}He ions and 2.5 MeV protons with information depth of about 1 and 20 μm, respectively. The ion beam hits the target at normal incidence. The scattering angle was 165°. Usually, a fluence between 5 μC and 20 μC was accumulated for a single spectrum. The size of the analysing spot was about 0.5–1.5 mm^2. To specify contamination proton induced X-ray emission (PIXE) was performed using 1.5 MeV protons.

The silicon concentration is evaluated by using the program SIMNRA [18] to generate the measured spectra by iterating the concentration and depth profile. The silicon concentrations used here refer to atomic concentrations. The information depths of a uniform Si doped graphites are listed in table 3. For obtaining a depth scale an atomic density for NS31 of 0.9×10^{29} at./m^3 was used (tab. 2). Changes in density due to concentration variations are neglected by the transformation from at./m^2 into μm.

	2.0 MeV ^{4}He			2.5 MeV ^{1}H		
energy of ^{28}Si edge (keV)	1135			2170		
energy of ^{12}C edge (keV)	511			1796		
energy of ^{2}D edge (keV)	–			284		
Si concentration (at.%)	10	25	50	10	25	50
maximal information depth of Si (μm)	1.92	1.71	1.47	27.2	24.4	20.7
information depth of Si signal at C edge (μm)	1.17	1.03	0.90	7.6	6.4	5.6
maximal information depth of C (μm)	0.93	0.81	0.70	22.4	20.3	17.4

TABLE 3: The information depths of backscattered 2.0 MeV ^{4}He and 2.5 MeV protons on a uniform Si doped graphite. The depths were obtained by using the program SIMNRA [18].

In order to determine the composition of the thin co-deposited layers, the deuterium amount in the deposited layers was quantified with the D(^{3}He,p)α nuclear reaction (NRA) at an incident energy of 0.79 MeV. Only a fluence of 1 μC was accumulated to minimise the driving out of deuterium by the ^{3}He ions. The protons from the nuclear reaction were detected with a large angle counter of about 145°. Afterwards the carbon, silicon and oxygen content at the same analysing position were quantified with backscattering (RBS) of 2.0 MeV ^{4}He ions (165°, 20-40 μC, 0.5 mm^2).

2.4 Ion bombardment

For the erosion measurements the Garching high current ion source for light ions [19] was adjusted to produce 3 or 6 keV mass separated ions, mostly D_3^+ ions. The ions were slowed down by biasing the target to a chosen impact energy in the range of 20 eV to 3 keV per deuterium atom. The

bombarded spots had sizes of between about 0.5 and 0.8 cm^2 depending on the impact energy. An ion current of between 50 μA and 100 μA was used corresponding to fluxes of about $1–4\times10^{19}$ $D^+/m^2/s$. The sputtering yield was determined by measuring the weight loss and the total ion charge. The applied fluences were between 0.1 and 5×10^{24} D^+/m^2.

In order to determine the chemical part of erosion the CD_4 production versus the target temperature was monitored and compared to those of pure carbon (pyrolytic graphite (HPG) from Union Carbide, USA). During the bombardment the temperature was increased in steps and held for 6 minutes to ensure steady state conditions. Degassing experiments after D_3^+ implantation were performed using thermal desorption spectroscopy (TDS) up to 1450 K with about 6 K/s linear heating rate. Information on the amount of retained D were obtained, calibrated with NRA measurement and compared to pyrolytic graphite.

3 Results

The 3D CFC NS31 shows a strong anisotropy of the thermal conductivity. An influence to the Si concentration and the sputtering yield from the orientation of the sample surface with respect to the high thermal conductivity direction was not observable in all our measurements.

3.1 Initial NS31 of delivery A

In SEM, four different areas of 0.01–1 mm^2 size could be characterized on the surface of initial NS31 (Fig. 1). The areas consists of pure graphite, big crystallites (30 μm) of Si or SiC, thin cut carbon fibres (6 μm diameter), and thick carbon fibres (30 μm diameter) with a smooth cover of Si or SiC, visible in holes due to manufacturing procedure (Fig. 1b–e). Due to the fibre structure, the material NS31 is inhomogeneous in the dimension of millimetres. Due to ion bombardment strong erosion profiles are created at the graphite areas with structures beneath 1 μm, the Si or SiC crystallites are rounded, and on all thick Si or SiC covered fibres crystallites (4–12 μm) have been grown.

The spot of the analysing ion beam is too small to average over the lateral inhomogeneity and to obtain a representative spectrum for a sample face. Therefore, for each face a series of spectra at different positions were averaged to obtain a representative spectrum (thick line in fig. 2a). In figure 2b the representative spectra for many initial faces for 2.0 MeV ^4He and the average over these are shown. The signal at the Si and C edge results from backscattering from surface atoms. The energy scale is an equivalent for a depth scale for each element separately; lowering the backscattering energy means increasing the depth. For comparison simulated spectra using the program SIMNRA [18] with different homogeneous mixtures of Si and C (5 at.% steps) are plotted in figure 2a. A simulated spectrum for 8 at.% Si and 92 at.% C agrees well with the average spectrum of the initial faces. The shape of each single measured spectrum for the initial surface could be reproduced by a homogeneous Si distribution in depth with laterally varying the Si concentration between 0 and 20 at. % Si (Fig. 2a). Averaging over one sample the variation of the Si concentration is reduced to 5–12 at. % Si (Fig. 2b).

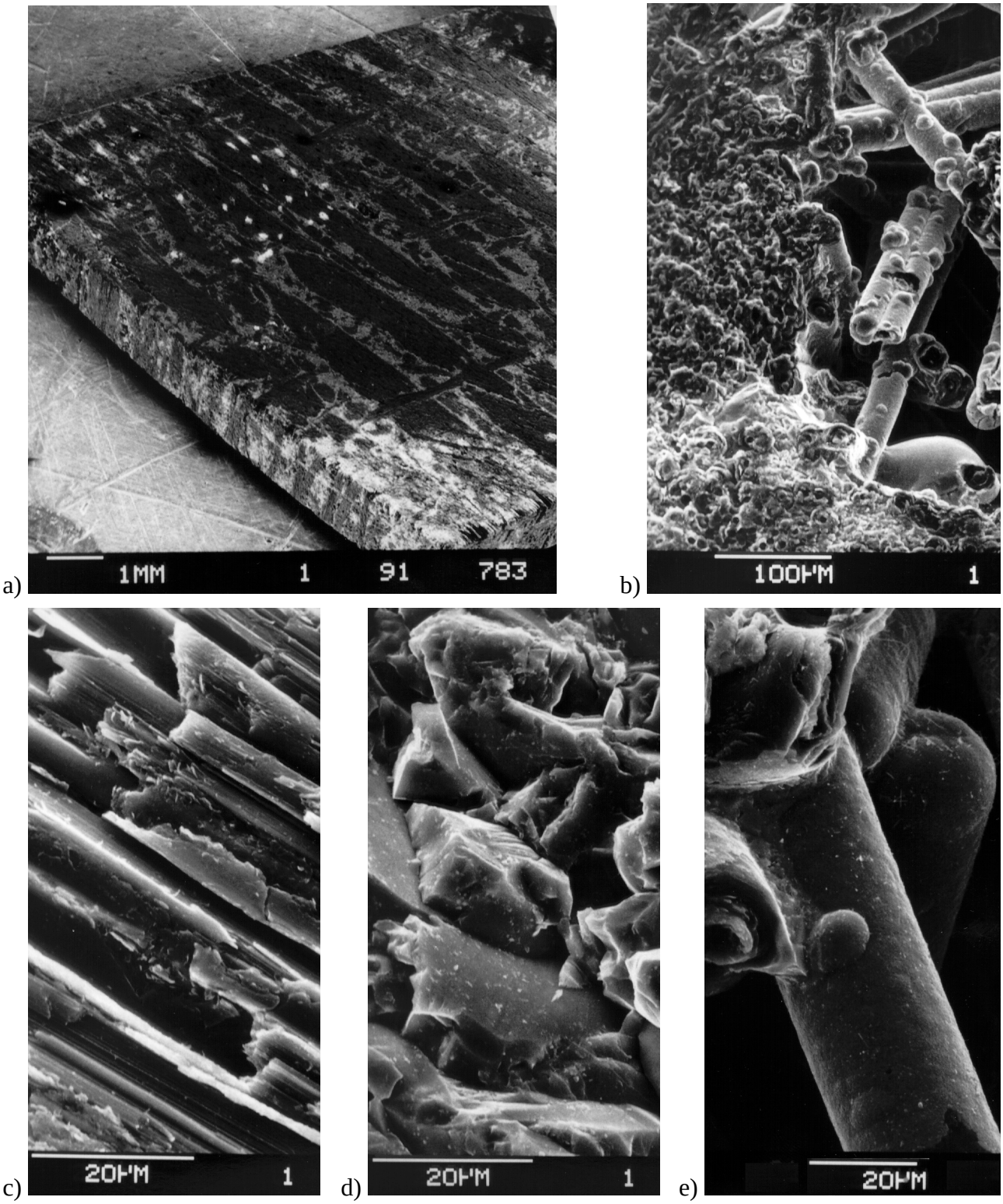

FIGURE 1: SEM pictures of initial NS31 of delivery A with X direction perpendicular to the surface; a) overview; b) thin carbon fibres (right) and thick carbon fibres with a smooth cover of Si or SiC (left); c) area of pure graphite; d) area of big crystallites of Si or SiC; e) thick carbon fibres with a smooth cover of Si or SiC.

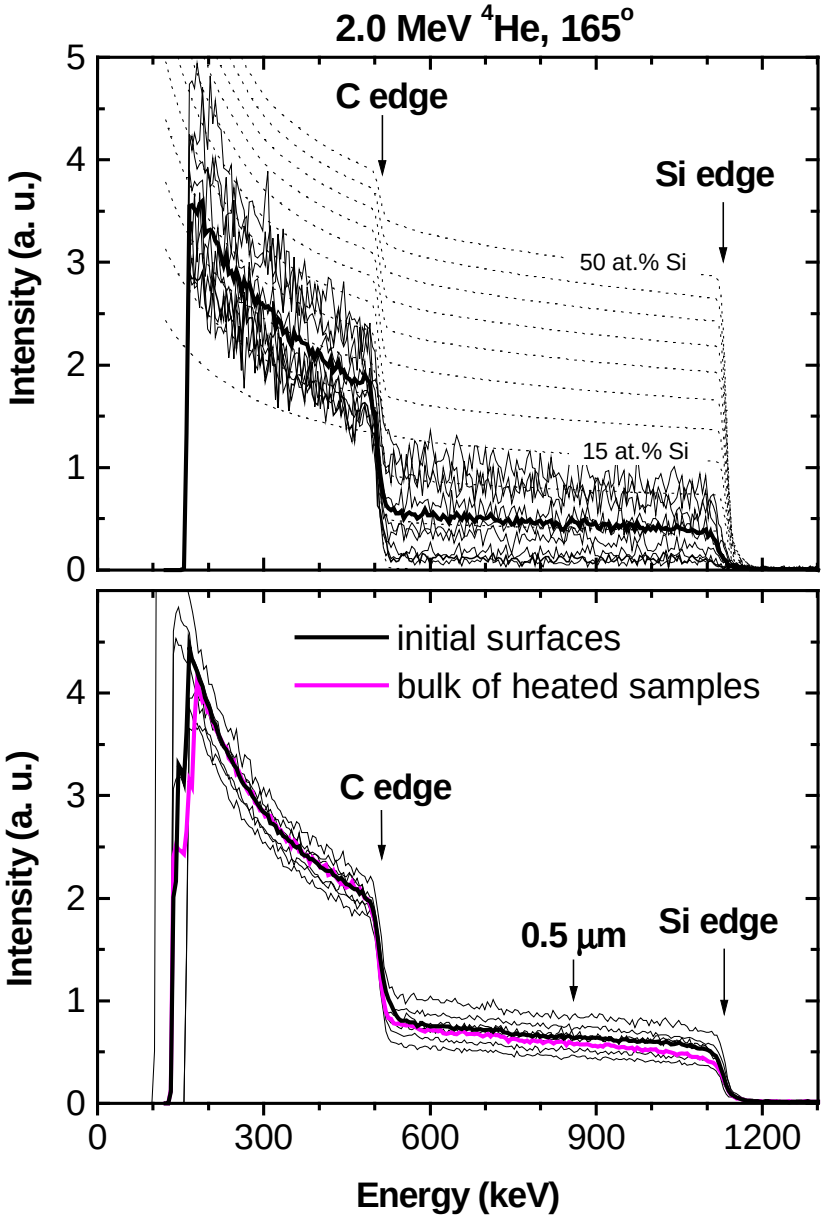

FIGURE 2 Top: Series of backscattering spectra of 2.0 MeV ^{4}He at different positions of an initial face (thin lines) and the representative spectrum (thick line) of this face. The dashed lines represent simulated spectra of homogeneously silicon doped carbon (between 0 and 50 at.% Si in 5 at.% steps); bottom: averaged spectrum (thick black line) over the representative spectrum of several initial samples (thin lines) of delivery A and the averaged spectrum of the bulk of several heated samples (thick grey line). The energy corresponding to the depth of about 0.5 μm for the silicon signal is marked.

For the determination of the sputtering yield from the weight loss measurements, the composition of the sputtered material has to be taken into account: It has been assumed that at high fluences the composition of eroded material is equal to the bulk composition and that this steady state is reached in our measurements. For initial faces 10 at.% Si in carbon was used.

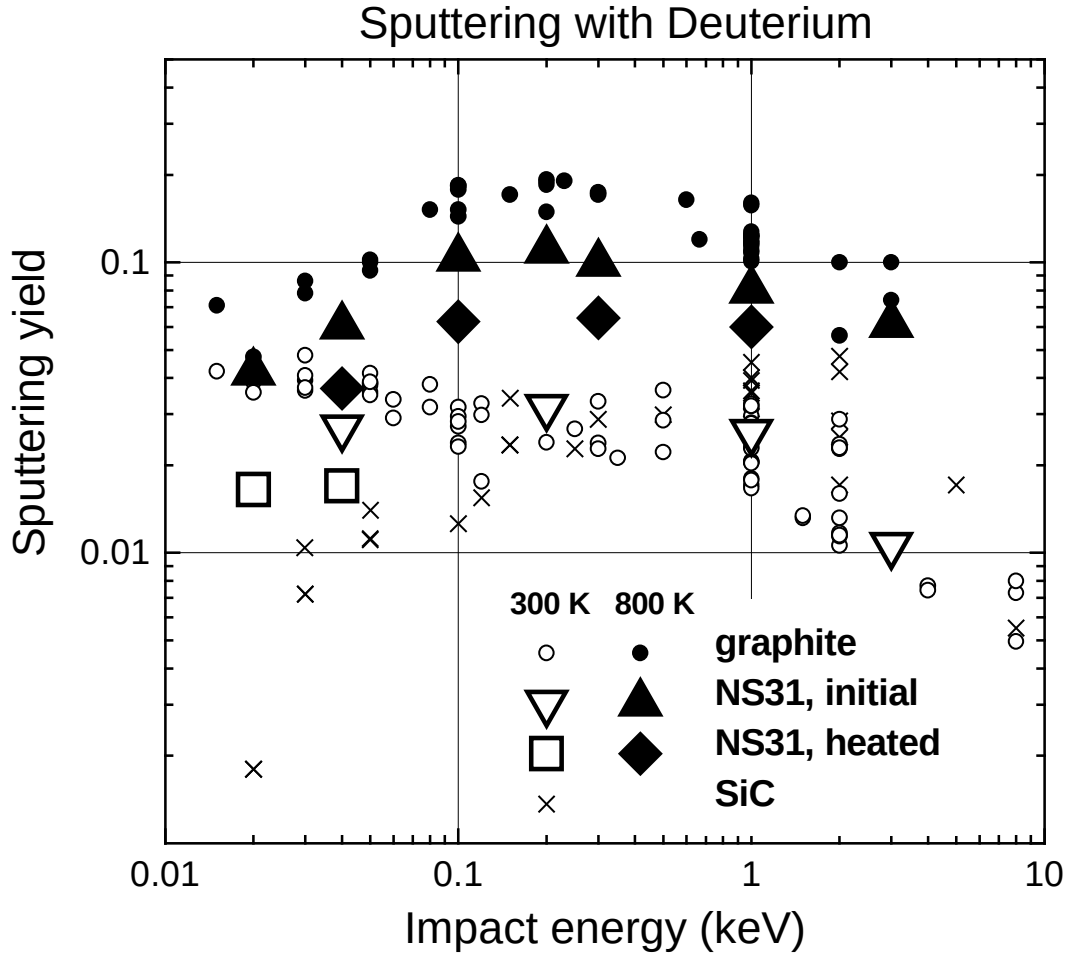

FIGURE 3: Sputtering yield data of pure graphite (circles) [20, 22], of SiC (crosses) [9], of initial faces (triangles), and of heated faces of NS31 of delivery A (squares / diamonds) for perpendicular incidence of deuterium versus impact energy. Open data points were measured at 300 K, filled ones around 800 K with fluxes of around 1–4×10^{19} D/m^2/s.

The temperature dependence of the sputtering yield of pyrolytic graphite and NS31 due to the dominant chemical erosion processes – the thermally activated hydrocarbon emission (Y_{therm}) [20, 21] – was measured. The maximum for both, graphite and NS31, was found at the same temperatures, at about 850 K for 200 eV deuterium and at about 700 K for 30 eV deuterium. To relate the yield of NS31 to those of graphite and silicon carbide [9, 20, 22], the measured yields of NS31, graphite, and SiC are plotted in figure 3 versus the impact energy. The measured yields of

NS31 are between the yield of graphite and silicon carbide. At around 800 K a reduction of a factor about 2 compared to graphite was obtained throughout the investigated energy range. At 300 K, below 100 eV the kinetic ejection of surface hydrocarbon complexes from a collisional energy transfer (Y_{surf}) exceeds the unavoidable physical sputtering [20, 21], which dominates the yield above 100 eV. Also this chemical erosion is reduced. The reduction is shown directly by the measured CD_4 production yield versus the target temperature for graphite and different samples of NS31 (Fig. 4). For the initial face (triangles), the results of the weight loss measurements at 1 keV and 30 eV were confirmed.

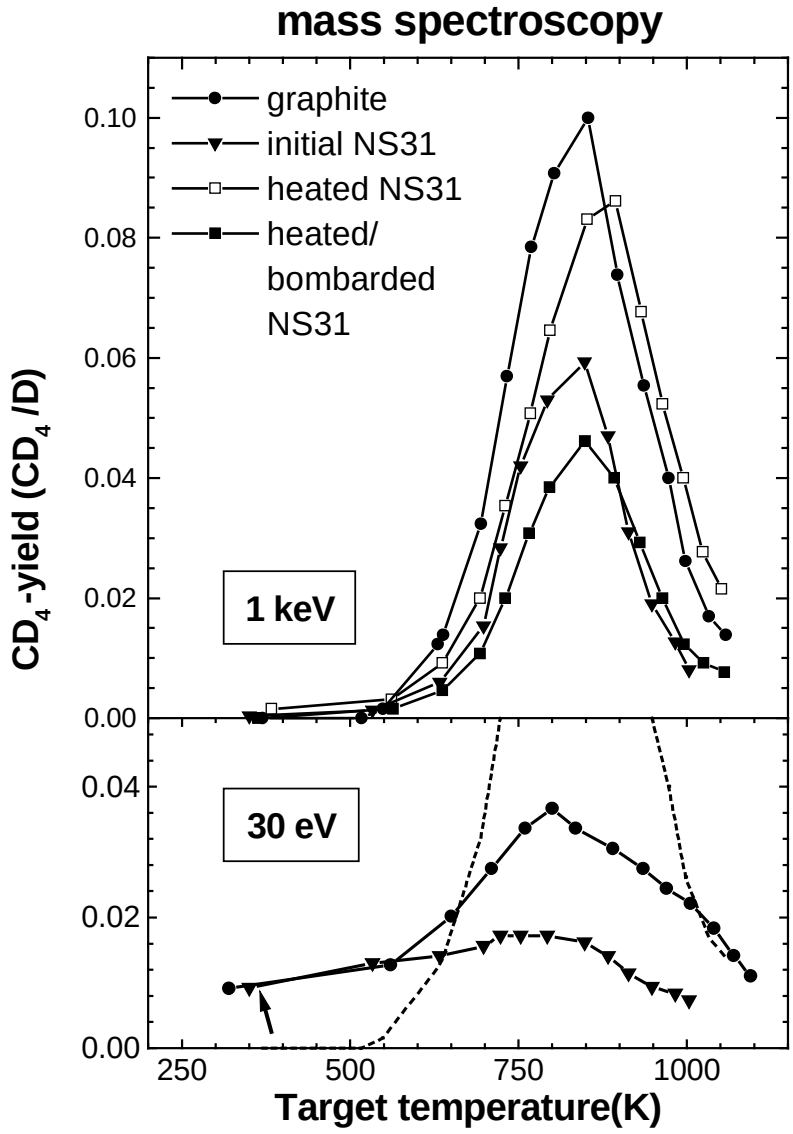

FIGURE 4: CD_4 production yield versus target temperature of pure graphite (circles), of an initial sample (triangles), of a freshly heated face (open squares), and of the heated face after a fluence of 2.5×10^{24} D/m^2 (solid squares).

In order to obtain information about the amount of retained deuterium after implantation, TDS measurements were performed. The shape of the TDS spectra of initial NS31 and pyrolytic graphite look similar (Fig. 5). The contribution of the silicon as inferred from measurements on SiC [23] is too small to be visible. The amount of retained D in NS31 – measured with TDS and NRA – did not completely saturate with fluence, a well known behaviour of porous graphite's and doped ones (Fig. 6) [23, 24]. This could be interpreted as the migration of deuterium into the bulk along grain boundaries and trapping beyond the implantation zone [25].

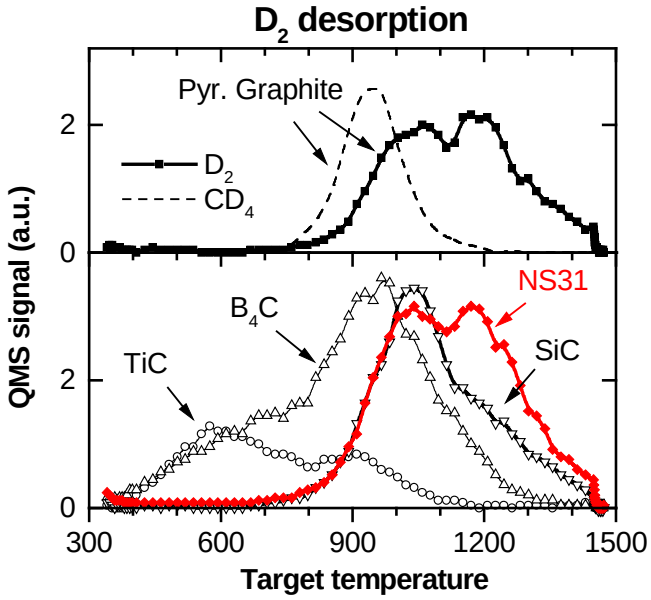

FIGURE 5: TDS spectra of D_2 molecules released from pyrolytic graphite, carbides (B_4C, SiC, TiC), and NS31 implanted at about 300 K with 1 keV per D and a fluence of 2.7×10^{22} D/m^2. The TDS spectrum of CD_4 molecules for pyrolytic graphite is shown as a dotted line. All spectra were recorded with a linear heating ramp of about 6 K/s.

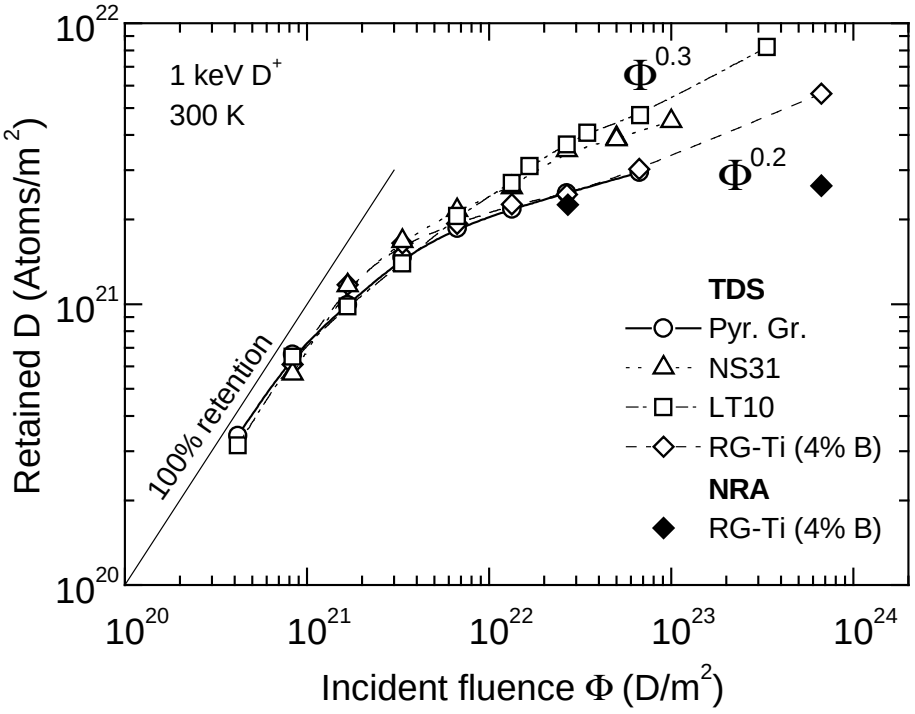

FIGURE 6: Fluence dependence of the retained amount of deuterium in pyrolytic graphite, LT10 (10 at.% titanium), Rg-Ti-91 (1.7 at.% titanium and 4 at.% boron) and NS31 for bombardment with 3 keV D_3^+ at room temperature. The retained amount was determined with NRA and TDS [23].

3.2 Heated NS31 of delivery A

Due to the first heating to 1800 K for 2 hours, a weight loss of about 1–5 % of 0.3 g samples has been observed together with a deposition of evaporated silicon on the walls of the heating chamber. During a second heat treatment the relative weight loss was less than 6×10^{-4}.

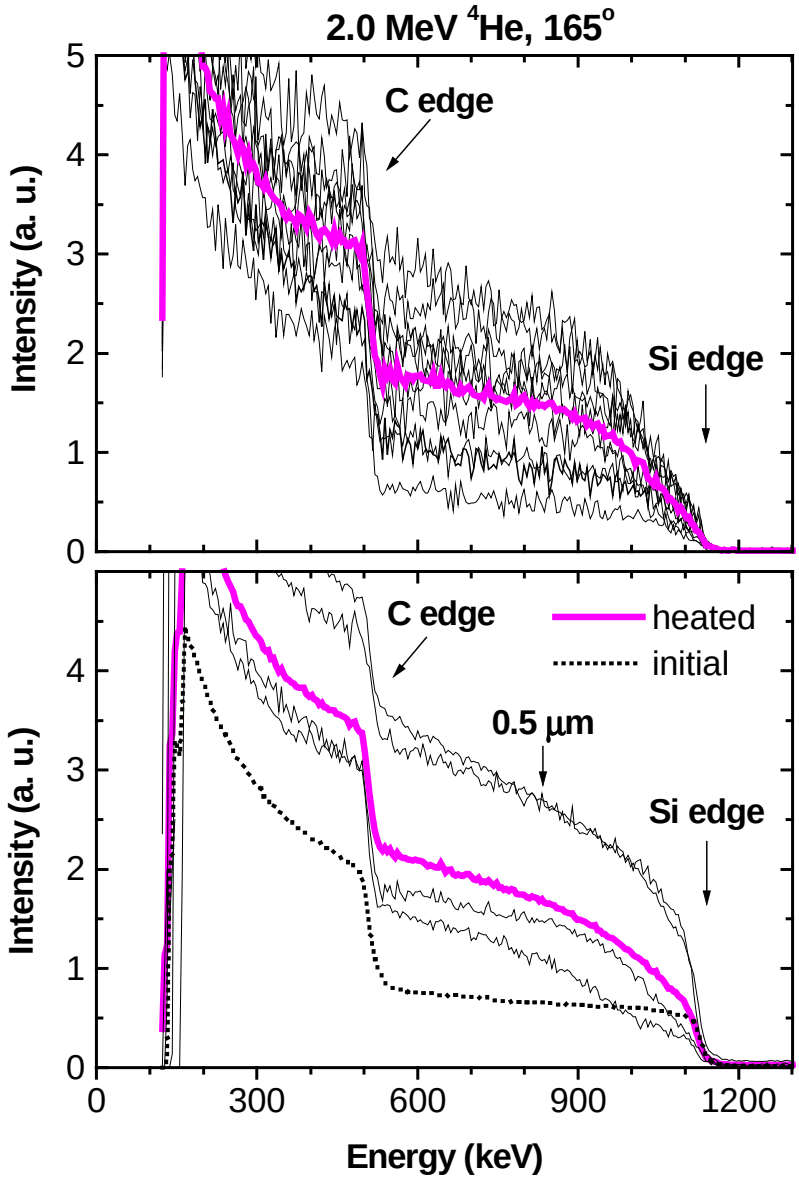

FIGURE 7: a) Series of backscattering spectra of 2.0 MeV ^{4}He at different positions of a heated face (thin lines) and the representative spectrum (thick line) of this face; b) averaged spectrum (thick line) over the representative spectra of several heated samples of delivery A (thin lines) and the averaged spectrum of several initial samples of delivery A (dotted line). The energy corresponding to the depth of about 0.5 µm for the silicon signal of initial faces is marked.

3.2.1 Surface of heated NS31

From the four different areas of initial faces visible in SEM, only the thick fibres are not modified by the heat treatment. They stay smooth. The other areas are sprinkled with small crystallites of Si or SiC (1–8 μm). After additional D_3^+ bombardment the concentration of the small crystallites was increased. Rounded Si or SiC crystallites and strong erosion profiles in the graphite in-between crystallites are visible. Every thick fibre is covered completely with rounded crystallites (4–12 μm).

In figure 7, each spectrum of a series of spectra at different positions, the representative spectrum of several heated samples as well as the average backscattering spectrum of several heated faces shows an increasing Si intensity below the Si edge. Such a shape of a 2.0 MeV ^{4}He backscattering spectrum can be explained by a Si profile starting with a silicon depletion near the surface and enrichment with depths. An increasing Si concentration with depth is also indicated by the EIXE measurements, where the intensity of the silicon EIXE signal on a heated face decreases with decreasing penetration depth (decreasing electron beam energy), while it was constant on initial and 'cut' faces. By iterating the concentration and depth profile in the program SIMNRA [18], the backscattered spectra are simulated. To obtain a depth scale for the profiles an atomic density for NS31 of 0.9×10^{29} at./m^3 was used neglecting changes in density. In a depth of around 0.5 μm, for some heated faces a big variation between 0 and 40 at.% Si at different positions was observed. For some other faces the variation was only between 40 and 50 at.% Si.

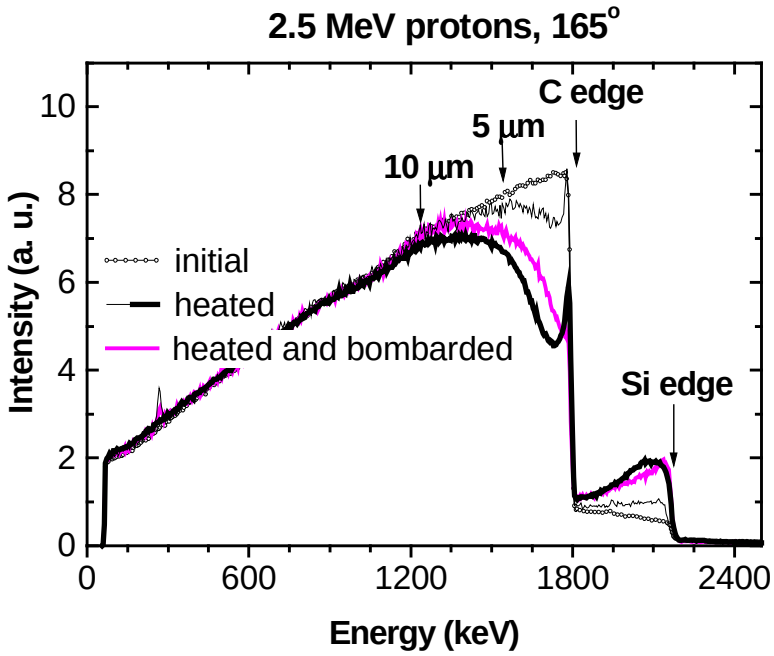

FIGURE 8: Representative backscattering spectra of 2.5 MeV protons of several different samples of delivery A: one initial (dotted line), two heated (thin and thick black line) before D bombardment and one heated face (grey line) after D bombardment with a fluence of 4.5×10^{24} D/m^2. The energy corresponding to the depth of about 5 μm and 10 μm for the silicon signal of initial faces is marked.

In the representative backscattering spectra of 2.5 MeV protons (Fig. 8), the Si depletion zone at the heated surface produces a narrow peak at the carbon edge. The dip in the carbon signal at around 1700 keV and the increase of the signal below the Si edge in comparison with a spectrum of an initial face characterize the Si enriched layer. From the comparison with simulated spectra, the thickness of the enrichment layer could be determined. It varies for the different face between around 5–10 μm. By deuterium bombardment the altered layer can be partly removed, as the missing peak at the C edge and the shift of the dip in the carbon signal and of the Si peak indicate (Fig. 8).

The sputtering yields are averaged values over the removed part of the Si profile. By measuring the CD_4 production of a freshly heated surface and after removing parts of the enrichment layer, it could be clearly shown that the chemical erosion decreases with increasing Si concentration (Fig. 4). For all impact energies the measured total sputtering yield for the heated surfaces is lower than for the initial NS31 (Fig. 3). A reduction of a factor 3 compared to graphite is reached.

In the TDS measurements no differences between heated surfaces and initial faces were observed, except that the shape of the TDS spectra shows an indication for a higher silicon contribution of the heated surfaces. The amount of retained D is the same.

3.2.2 Bulk of heated NS31

A freshly cut face of a heated sample looks like an initial face with all four features clearly visible in SEM (Fig. 9). The only noticeable change due to the heat treatment is the roughening of the coating of the thick fibres with structures below 1 μm size. In the ion beam analysis the lateral distribution of the silicon, the shape of the single measured spectra, and the average spectrum of several 'cut' faces (Fig. 2b) could not be distinct from those of the initial faces. Also in the determination of the sputtering yield no difference was observable.

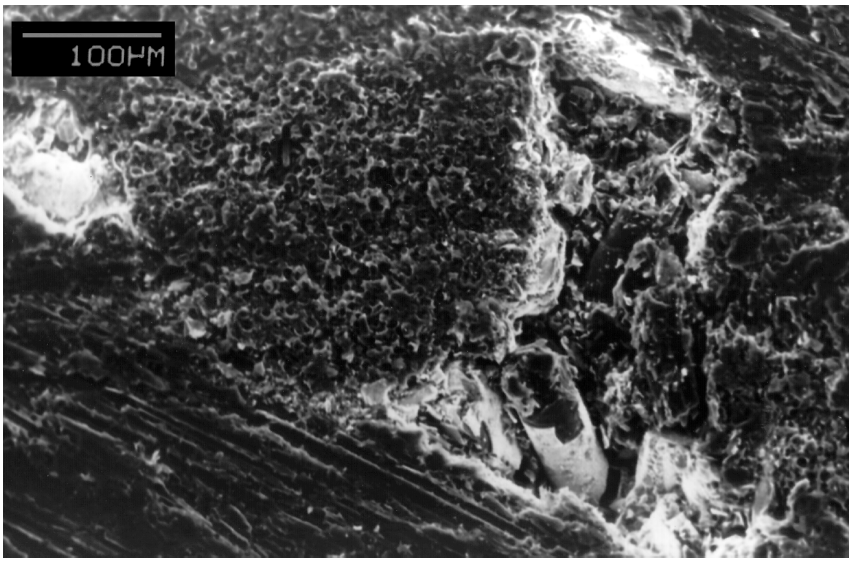

FIGURE 9: SEM picture of the bulk of heated NS31 of delivery A with Y direction perpendicular to the surface. All four different areas of the initial NS31 could be recognised (left bottom: pure graphite area; bright spots at left top and at right bottom: small areas of Si or SiC crystallites; middle left: bunch of thin carbon fibre; middle right: thick carbon fibre with cover of Si or SiC).

Heating a 'cut' face a second time to 1800 K for 2 hours, no enrichment layer occurs and only the depletion zone is created. Such a depletion is a well known behaviour of Si doped graphite's due to evaporation of Si [26, 27].

3.3 Initial NS31 of delivery B and C

The material of the deliveries B and C was only investigated in respect to the dopant distribution of the initial material. In figure 10 the average spectra over large areas of several initial samples of delivery B (thick grey line) and delivery C (thick black line) are shown. For comparison the average spectrum over several initial samples of delivery A (Fig. 2) and simulated spectra of homogeneously silicon doped carbon between 0 and 10 at. % Si are shown, too.

The average spectrum of delivery C is nearly covered by the average spectrum of delivery A. The averaged silicon concentration is about 8 at. %. Also, in the variation of the silicon concentration of the single spectra (0–20 at. % Si) both deliveries are comparable. On some samples metal impurities were observed, which could be assigned to iron or nickel. The accumulation of the impurities near the surface (manifested in the peak below 1.5 MeV) gives a hint that the impurities are implemented due to the cutting procedure.

The material of delivery B has a much lower silicon concentration of only about 1 at. %. This material misses the specification of NS31 (Tab. 2).

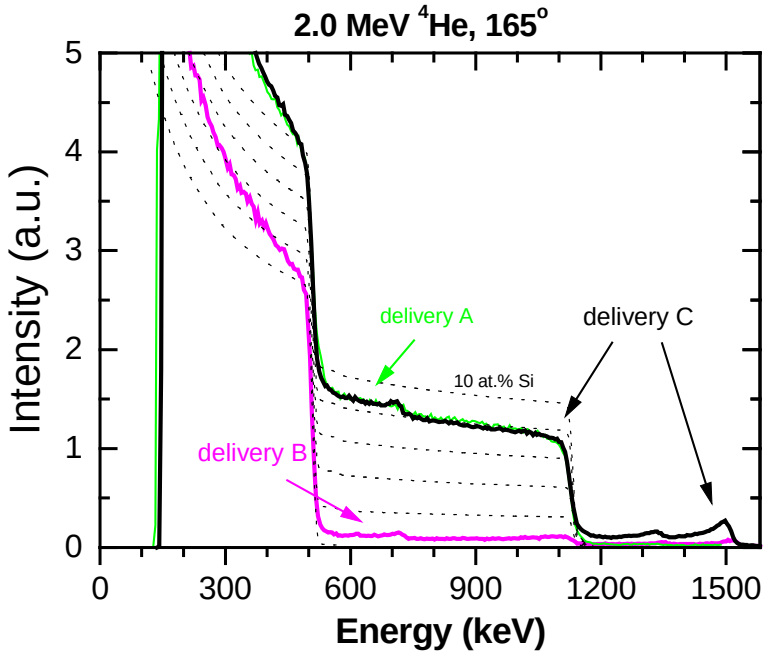

FIGURE 10: Average spectra over the representative spectra of several initial samples of delivery B (thick grey line, 90 single spectra) and delivery C (thick black line, 147 single spectra). The average spectrum of delivery A (Fig. 2, thin grey line, 134 single spectra) is nearly covered by the spectrum of delivery C. The dashed lines represent simulated spectra of homogeneously silicon doped carbon (between 0 and 10 at.% Si in 2 at.% steps).

3.4 Co-deposition of NS31 with deuterium

In figure 11 the result of the determination of the composition of a co-deposited layer from a NS31 target is shown. The content of C, D and Si increases linear with the thickness of the layer ((C+Si) atoms). The ratio of D per (C+Si) atoms is about 0.6. This ratio is a little higher than for pure carbon and reflects the general trend of the dependence of D concentration on the composition in the C/Si mixed system which has a maximum of about 0.7 D per (C+Si) at ratio C per Si around 1 [28].

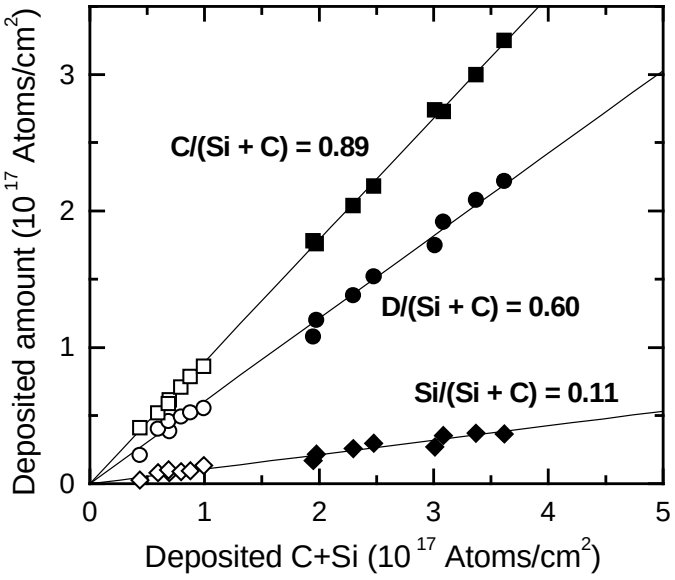

FIGURE 11: Amount of D (circles), C (squares), and Si (diamonds) versus total amount of re-deposited (C+Si) target atoms of a NS31 sample of delivery A. The sample was bombarded with 3 keV D_3^+ ions and the layer was deposited at room temperature.

In order to obtain the temperature dependence of the D concentration in co-deposited layers, the NS31 target and the collector plate were heated to about the same temperature. Figure 12 summarises the decrease of the ratio of D atoms per (C+Si) atoms with increasing temperature. For comparison, data for the pure carbon material N112 [28] and data taken from [29] for D implantation in C at room temperature with subsequent annealing and for D implantation in C at elevated temperatures are shown. For the co-deposited layers the D concentration is always much lower than the value found for room temperature implantation in C and subsequent annealing, indicating an ion enhanced release during deposition. However, the values are higher than expected from implantation at elevated temperatures. This may due to the large contribution of reflected D atoms with energies much lower than the primary ion energy.

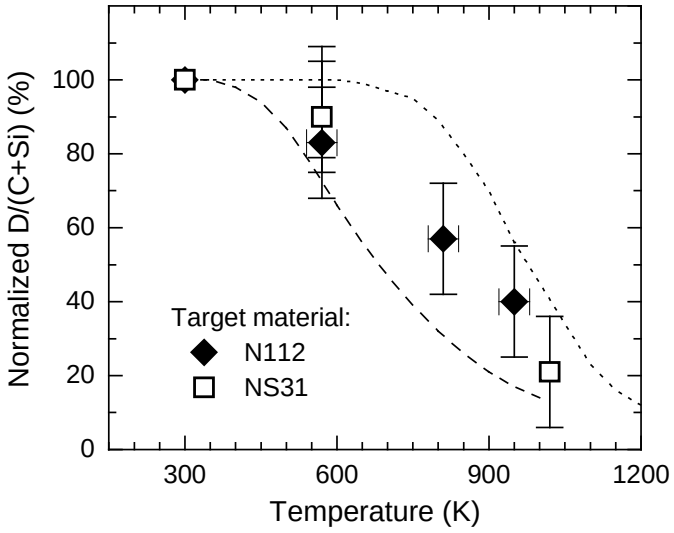

FIGURE 12: Ratio of D atoms to re-deposited target atoms for NS31 (squares) versus the temperature of the collector plate. For comparison, data for the pure carbon material N112 (diamonds) [28] and data taken from [29] for D implantations in C at room temperature with subsequent annealing (dotted line) and for D implantation in C at elevated temperatures (dashed line) are shown. The ratios are normalised to the ratio at room temperature.

3.5 Mock-up tile

3.3.1 Surface of the mock-up tile

In SEM, the surface of the mock-up tile show strong erosion profiles with structure of a size of around 1 μm, also on the thick carbon fibres. Due to the smallness of the structures it is not possible to distinguish between graphite areas and crystallites. With EIXE areas of pure carbon could be found, as well as areas with high amounts of Si. But additional, a tungsten signal was observed in EIXE as well as in PIXE. No tungsten pellets could be resolved on the surface in SEM. Due to the high mass of tungsten, these contaminations lead to disturbing signals in the backscattering spectra extending to the energies of the Si edge and below. So, if the whole signal just above the C edge is attributed to silicon, the Si concentration could be estimated to below 3 at.% in the surface layer of at least 5 μm. Tungsten concentrations up to 4 at.% W were observed at the surface with decreasing concentration with increasing depth. The tungsten on the mock-up tile originates from neighbouring tungsten mock-up tiles during the heat load test. Due to the high tungsten contamination no sputtering and TDS measurements of the mock-up tile were performed.

3.3.2 Bulk of mock-up tiles

In contrast to the surface, for the bulk of the mock-up tile the ion beam analysis and REM do not provide any difference to initial or 'cut' faces. So, the results of the initial faces could relate to the bulk of the mock-up tile.

4 Conclusion

The silicon concentration at the surface of the as received NS31 of the delivery A (1996) is altered after heating to elevated temperatures. The observed results of SEM and ion beam analysis imply that during the heat treatment to 1800 K for 2 hours, free silicon segregates to the surface and enriches a layer of 5–10 μm thickness. Silicon carbide is formed during this process. With extending heating time, a fraction of the silicon from the surfaces of the SiC crystallites evaporates. The observed profiles reflect the average over the distribution of the crystallites of μm size and the depletion of the surface in silicon. The silicon concentration in the enrichment layer depends on the non-uniform characteristics of the received NS31. In particular, the distribution of free silicon causes different degrees of enrichment. It is interesting to note, that no further silicon segregation has been observed in NS31 after additional heat treatments.

During the high heat load (18 MW/m^2) of mock-up tiles, surface temperatures up to 2300 K have been reached. A rapid evaporation of silicon caused a depletion of silicon in a surface layer of more than 5 μm thickness.

The distribution of the SiC crystallites influences the sputtering yield. A comparison of initial, heated, and heated/bombarded faces shows a reduction of the sputtering yield increases with increasing silicon concentration. Overall, a reduction by a factor of about 3 compared to graphite has been found for heated/bombarded NS31 samples of the delivery A. In addition, a reduction of the chemical erosion due to the flux and energy dependence should be kept in mind [20, 21, 30-34].

In respect to the tritium inventory, no significant difference in the implantation behaviour of deuterium into NS31 compared to pure carbon materials has been observed. For the co-deposition of deuterium with the re-deposited material of eroded NS31 a ratio of about 0.6 D per (C+Si) atoms were measured. This ratio is a little higher than for pure carbon.

In respect of the silicon distribution the material of the delivery C (1998) is like the material of delivery A with an average silicon concentration of about 8 at. %.

The material of the delivery B (1997) fails the specification. It has only an average silicon concentration of about 1 at. %.

Acknowledgements

The authors would like to thank J. Gruber (Institut Dr. Ing. H. Klingele, Adelgundenstr. 8, 80538 München, Germany), S. Bassen, W. Ottenberger, M. Mayer and H. Plank (IPP) for the experimental performance and assistance and C.H. Wu (NET) and G. Vieider (NET) for useful discussion.

Literature

[1] J. Roth, E. Vietzke and A.A. Haasz in: *Atomic and Plasma-Material Interaction Data for Fusion*, Vol 1 of *Nuclear Fusion, Special Issue*, (IAEA, Vienna), (1991) 63.

[2] C. Garcia-Rosales, E. Gauthier, J. Roth, R. Schwörer and W. Eckstein, J. Nucl. Mater. 189 (1992) 1.

[3] C. Garcia-Rosales and J. Roth, J. Nucl. Mater. 196–198 (1992) 573.

[4] V.K. Alimov, R. Schwörer, B.M.U. Scherzer and J. Roth, J. Nucl. Mater. 187 (1992) 191.

[5] C. Garcia-Rosales, J. Roth and R. Behrisch, J. Nucl. Mater. 212–215 (1994) 1211.

[6] A.Y.K. Chen, A.A. Haasz and J.W. Davis, J. Nucl. Mater. 227 (1995) 66.

[7] P. Franzen, A.A. Haasz and J.W. Davis, J. Nucl. Mater. 226 (1995) 15.

[8] R. Schwörer and J. Roth, J. Appl. Phys. 77 (1995) 3812.

[9] H. Plank, R. Schwörer and J. Roth, Surf. Coat. Technol. 83 (1996) 93.

[10] H. Plank, R. Schwörer and J. Roth, Nucl. Instr. Meth B 111 (1996) 63.

[11] J. Roth, H. Plank and R. Schwörer, Physica Scripta T64 (1996) 67.

[12] R. Schwörer, H. Plank and J. Roth, J. Nucl. Mater. 230 (1996) 208.

[13] M. Balden, J. Roth and C.H. Wu, accepted to publication in J. Nucl. Mater.

[14] M. Balden, *Thermal stability and erosion of the silicon doped CFC material NS31*, Tech. Rep. IPP 9/112, Max-Planck-Institut für Plasmaphysik, (1997).

[15] SEP, Final Report NS31, Tech. Rep., France, (1996).

[16] G. Vieider et.al., *Overviewof EU small scale mock-up tests for ITER high heat flux components*, in: *Proceedings of 4th ISFNT*, Tokyo, (1997).

[17] Institut Dr. Ing. H. Klingele, Adelgundenstr. 8, 80538 München.

[18] M. Mayer, *SIMNRA User's Guide*, Tech. Rep. IPP9/113, Max-Planck-Institut für Plasmaphysik, Garching, (1997).

[19] W. Eckstein, C. Garcia-Rosales, J. Roth and W. Ottenberger, *Sputtering Data*, Tech. Rep. IPP 9/82, Max-Planck-Institut für Plasmaphysik, (1993).

[20] J. Roth and C. Garcia-Rosales, Nucl. Fusion 36 (1996) 1647.

[21] J. Roth and C. Garcia-Rosales, Nucl. Fusion 37 (1997) 897.

[22] M. Balden accepted for publication in Physica Scripta.

[23] M. Mayer, M. Balden and R. Behrisch, J. Nucl. Mater. 252 (1998) 55.

[24] A.A. Haasz and J.W. Davis, J. Nucl. Mater. 209 (1994) 155.

[25] A.A. Haasz, P.Franzen, J.W. Davis, S. Chiu and C.S. Pitcher, J. Appl. Phys. 77 (1995) 66.

[26] J. Roth, J. Bohdansky and J.B. Roberto, J. Nucl. Mater. 128&129 (1984) 534.

[27] I. Fujita et.al., J. Nucl. Mater. 241–243 (1997) 1185.

[28] M. Balden and J. Roth, J. Nucl. Mater. in press (13th PSI).

[29] W. Möller, J. Nucl, Mater. 162-164 (1989) 138.

[30] J. Roth, J. Nucl. Mater. in press (13th PSI).

[31] H. Grote, W. Bohmeyer, H.-D. Reiner, T. Fuchs, P. Kornejew and J. Steinbrink, J. Nucl. Mater. 241–243 (1997) 1152.

[32] H. Grote et al., J. Nucl. Mater. in press (13th PSI).

[33] A. Kallenbach, A. Thoma, A. Bard, K.H. Behringer, K. Schmidtmann, M. Weinlich and ASDEX Upgrade Team, Nuclear Fusion 38 (1998) 1097.

[34] A. Kallenbach et al., J. Nucl. Mater. in press (13th PSI).

Appendix B: Delivery information and cutting plans of both used blocks (No. 3 and 33)

NS31	OD : AE 45638E000 Lot : OR 2369560	
DEROG. N°	0084993	0085410

Block N°	**Schnittplan cutting plan**	**PAN length [mm]**	**needling width [mm]**	**pitch height [mm]**	**mass [g]**	**density [g/cm³]**
3	e	65,22	50,28	20,36	134,3	2,01
7	-	65,2	50,25	20,3	134,8	203
13	c	65,2	50,37	20,35	136,4	2,04
33	d	65,43	50,45	20,14	137,9	2,07
38	f	65,44	50,2	20,14	137,2	2,07

Schnittplan e
-N°3-

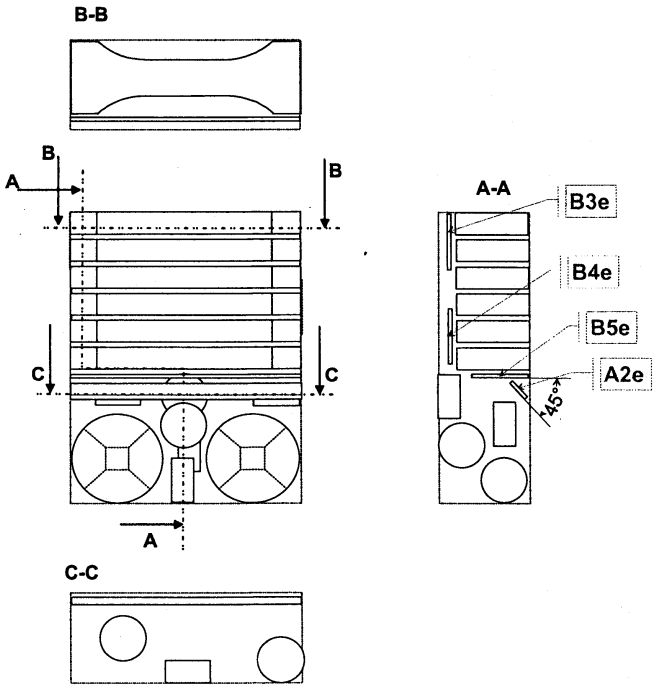

Schnittplan d
-N°33-

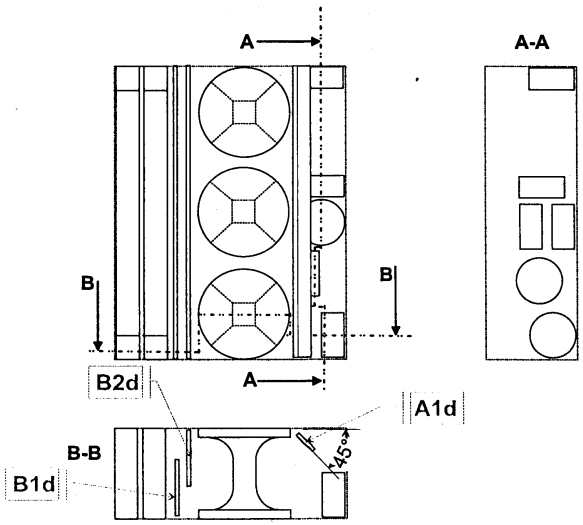

Appendix C: Information depth and conversion of intensity to concentration

A backscattering spectrum contains information about the depth distribution of the elements. The backscattering energy corresponds to the masses of the scattering partners and the composition of the passed material on the way in and out of the detected backscattered ion. For each element a maximal backscattering energy exists ("edge") and is determined by the kinematics, i.e. by the impacting energy and masses of the scattering target atom and the ion. At this energy the depth scale for the element starts. The signal height at that energy is correlated to the concentration of the element at the surface. An information depth for any backscattering energy can be defined if the composition is known or evaluated from the spectrum.

The information depths of **uniform** Si-doped graphite are calculated with the program SIMNRA [1]. For some interesting backscattering energies the information depth for Si and O are listed in tables **C1a, b**, and **c**.

The natural unit for depth in ion beam analysis is at./m^2. Changes in density due to concentration variations are neglected in the transformation from at./m^2 into μm. The atomic density for an 8 at.% Si-doped graphite, NS31 (left numbers), as well as for the atomic density of graphite, SiC, and silicon (right numbers in italic) were used to obtain the information depth for different energies in the backscattering spectra (Tab. **C1a**, **b**, and **c**).

For a uniform Si-doped graphite, the intensity (I) for the backscattering energy of 830 and 1200 keV for the 2.0 MeV ^{4}He and 1.5 MeV ^{1}H beam were calculated. They can be fitted by a quadratic dependence on the Si concentration (c_{Si}):

$$I = A\, c_{Si}^2 + B\, c_{Si}$$

The fitting constants A and B are given in table **C2**. From the measured spectra the accumulated intensity for the backscattering energy around 830 and 1200 keV were taken and normalised to an energy interval of 1 eV and a fluence of 1 μC. Then the Si concentration was calculated using the above given equation. Figure **C3** shows the quadratic dependence of the intensity on the Si concentration.

***TABLE C1a**: Information depth for **2.0 MeV ^{4}Helium** in Si-doped graphite backscattered at **silicon** atoms in different materials. Left numbers are obtained with a fixed atomic density of 8.9×10^{28} at/m^3 while right numbers (italic) are obtained with the given atomic density of the respective row.*

c_{Si} [at.%]	Specific density [g/cm^3]	Atomic density [10^{28} at./m^3]	830 keV: analysing depth [µm]		511 keV: depth of C edge [µm]		100 keV: maximal depth [µm]	
0	2.26	11.0	0.6	*0.5*	1.2	*1.0*	2.1	*1.7*
8	2.00	**8.9**	0.6		1.2		2.0	
25			0.5		1		1.9	
50	3.2	9.6	0.5	*0.4*	0.9	*0.8*	1.5	*1.4*
100	2.33	4.9	0.4	*0.7*	0.7	*1.3*	1.2	*2.1*

***TABLE C1b**: Information depth for **1.5 MeV protons** in Si-doped graphite backscattered at **silicon** atoms in different materials. Left numbers are obtained with a fixed atomic density of 8.9×10^{28} at/m^3 while right numbers (italic) are obtained with the given atomic density of the respective row.*

c_{Si} [at.%]	Specific density [g/cm^3]	Atomic density [10^{28} at./m^3]	1200 keV: analysing depth [µm]		1078 keV: depth of C edge [µm]		100 keV: maximal depth [µm]	
0	2.26	11.0	1.6	*1.3*	3.1	*2.5*	12.6	*9.9*
8	2.00	**8.9**	1.5		3.0		11.7	
25			1.4		2.7		10.5	
50	3.2	9.6	1.2	*1.1*	2.4	*2.2*	9.1	*8.4*
100	2.33	4.9	0.9	*1.6*	1.9	*3.4*	7.3	*12.9*

***TABLE C1c**: Information depth for **1.5 MeV protons** Si-doped graphite backscattered at **oxygen** atoms in different materials. Left numbers are obtained with a fixed atomic density of 8.9×10^{28} at/m^3 while right numbers (italic) are obtained with the given atomic density of the respective row.*

material	c_{Si} [at.%]	Specific density [g/cm^3]	Atomic density [10^{28} at./m^3]	1040 keV: analysing depth [µm]
C	0	2.26	11.0	0.6 *0.4*
NS31	8	2.00	**8.9**	0.5 *0.5*
SiC	50	3.2	9.6	0.3 *0.3*
Si	100	2.33	4.9	0.3 *0.5*
SiO_2	33	2.2	6.6	0.5 *0.6*

***TABLE C2**: Constants for quadratic dependence of intensity on Si concentration ($I=A\ c_{Si}^2 + B\ c_{Si}$) for the backscattering energy of 830 and 1200 keV for the 2.0 MeV ^{4}He and 1.5 MeV ^{1}H beam, respectively.*

Constant [counts/keV/µC]	2.0 MeV ^{4}He	1.5 MeV ^{1}H
A	-0.0017	-0.0060
B	0.35	1.10

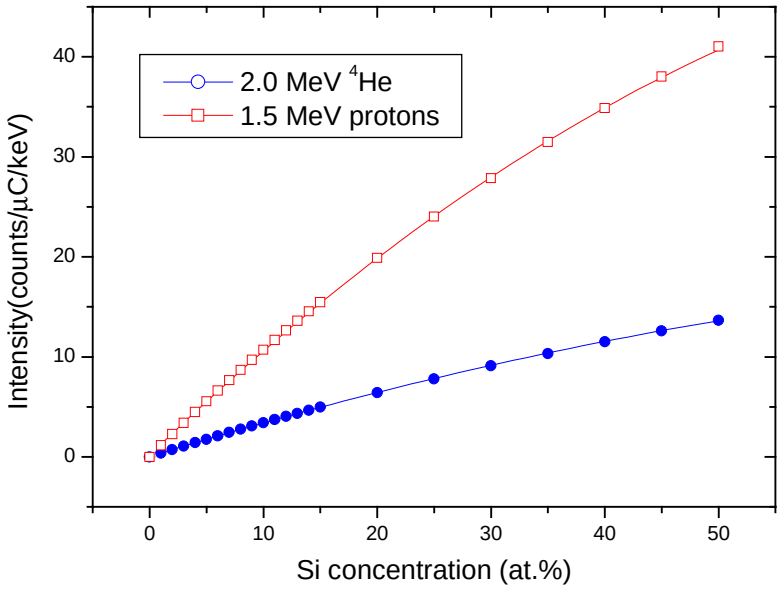

***FIGURE C3**: The quadratic dependence of the intensity on the Si concentration ($I=A\ c_{Si}^2 + B\ c_{Si}$) for the backscattering energy of 830 and 1200 keV for the 2.0 MeV ^{4}He and 1.5 MeV ^{1}H beam, respectively.*

Appendix D: Averaging of spectra

To achieve one average spectrum representative for the material NS31 of the delivery 2004 for each analysing ion type, He and proton, three different strategies can be followed:

Strategy **A**: Average all spectra arithmetically, i.e. using each single spectrum weighted by its analysing area. The total investigated area with Helium ions and protons was about 380 and 690 mm^2, respectively.

Strategy **B**: Taking the average spectra for each line scan and then arithmetically average these spectra.

Strategy **C**: Creating one average spectrum for each specimen and then average these spectra arithmetically.

Figure **D1** shows the spectra generated by these three averaging strategies.

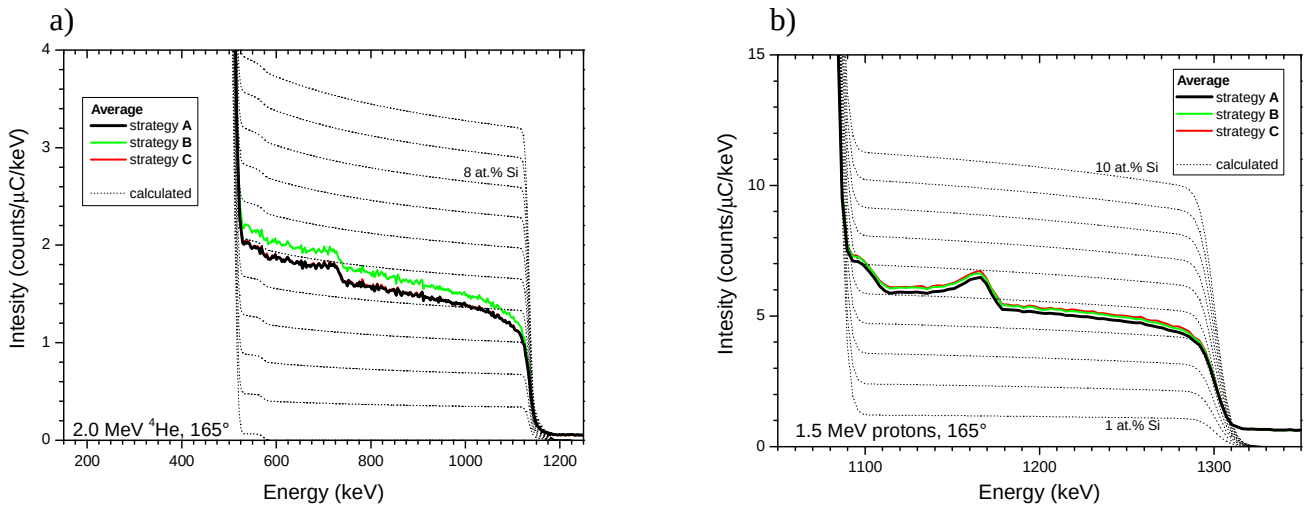

***FIGURE D1**: Average spectra generated by the three different strategies for a) ^{4}He ions and b) protons. The Si concentration of the calculated spectra varies stepwise by 1 at.% Si.*

Appendix E: XRD pattern of Si, SiC, and C as well as the analysing area

The XRD pattern of Si, SiC, and C are given in table **E1**, **E2,** and **E3**, respectively. The pattern are taken form the PDF data base [2]. The calculated analysing areas for the respective scattering angle are given, too.

TABLE E1*: Scattering angles for the low indexed X-ray diffraction peaks of* ***silicon*** *(PDF #27 1402 [2]) and the correlated analysing area of a d=2 mm collimated X-ray beam (d/tan* θ*).*

Indices (hkl)	Scattering angle 2 θ	Spot area (mm)
111	28.44°	8.1
220	47.3°	5.0
311	56.1°	4.3
400	69.1°	3.5
331	76.38°	3.2
422	88.0°	2.9
511	94.95°	2.7
440	106.7°	2.5
531	114.1°	2.4
620	127.5°	2.2
533	136.9°	2.2

***TABLE E2**: Scattering angles for the low indexed X-ray diffraction peaks of **SiC** (PDF #29 1129 [2]) and the correlated analysing area of a 2 mm collimated X-ray beam (d/tan θ).*

Indices (hkl)	Scattering angle 2 θ	Spot area (mm)
111	35.6°	6.5
200	41.4°	5.7
220	60.0°	4.0
311	71.8°	3.4
222	75.6°	3.3
400	90.1°	2.8
331	100.9°	2.6
420	104.5°	2.5
542	120.1°	2.3
551	133.6°	2.2

***TABLE E3**: Scattering angles for the low indexed X-ray diffraction peaks of graphite (PDF #41 1487 [2]) and the correlated analysing area of a d=2 mm collimated X-ray beam (d/tan θ).*

Indices (hkl)	Scattering angle 2 θ	Spot area (mm)
002	26.4	8.8
100	42.3	5.5
101	44.4	5.3
102	50.5	4.7
004	54.6	4.4
103	59.7	4.0
110	77.3	3.2
112	83.3	3.0
006	86.9	2.9
201	93.7	2.7

Appendix F: Used heating equipment

The used equipment for the heat treatment are given in figure **F1**. The glass tube is strongly coated by the evaporated material from the specimen **B2d #5**.

a) *b)* *c)*

FIGURE F1*: a) Overview image of the heating set-up with induction generator, water cooled coil and glass tube with vacuum pumping station. b) Detail image with the graphite crucible and the specimen* ***B2d #5*** *after the heating at 1700 K for 10 minutes. c) Detail image of the crucible on its Alumina holder after moving out of the induction coil. The side view for the micro pyrometer was not disturbed by the coating originated from the specimen* ***B2d #5*** *during its 10 minute heating at 1700 K.*

Appendix G: Lateral variation of Si concentration of NS31 of delivery 1996 and 2004

The figure **G1** shows the lateral variation of the silicon concentration at a depth of around 0.6 μm for each single spectrum of the different lateral scans, i.e. different specimen. The silicon concentration was obtained by using a comparison of the count rate at the backscattered energy of 830 keV generated by a 2.0 MeV ^{4}Helium ion beam and of spectra simulated by the program SIMNRA [1]. The labelled names represent different specimens. This figure is taken from [3].

In figure **G2** the same data are shown as in figure 3, but they are smoothed oven 10 data point. The data in Fig. **G2** mostly represent data for an area of 1x10 mm^2. No significant increase or decrease of the Si concentration at the end of the specimens is detectable.

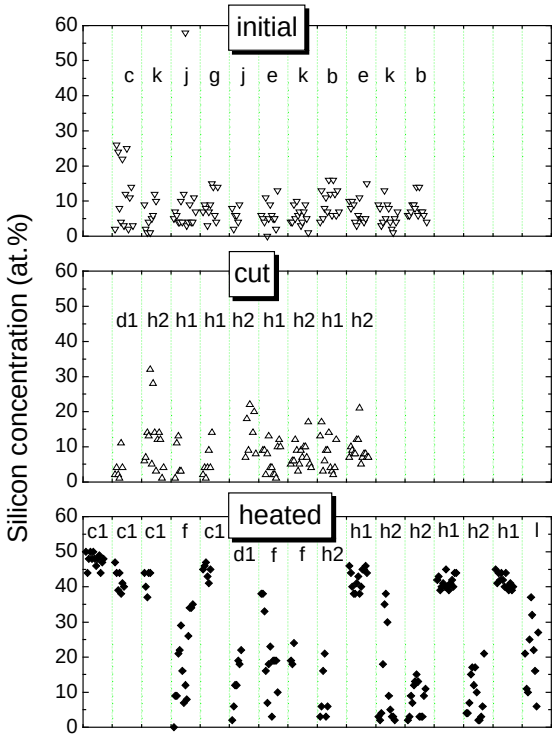

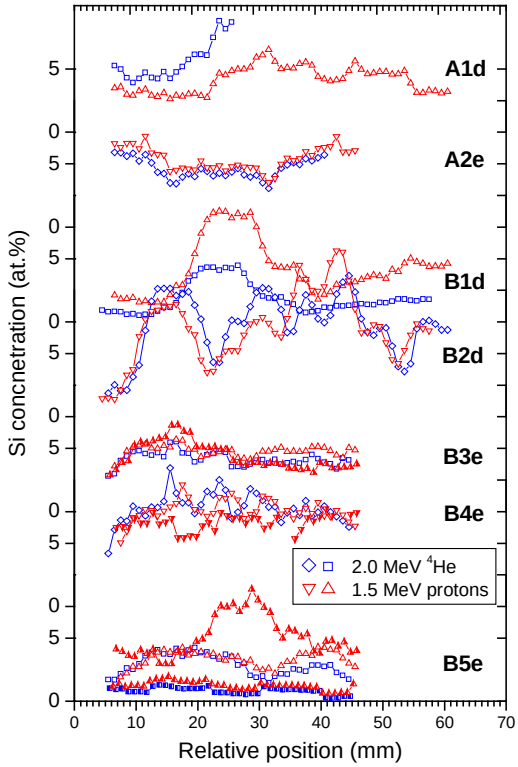

***FIGURE G1**: Si concentration of different specimen of NS31 of the delivery 1996. Some of the specimens were heated for 2 hours at 1800 K (h: heated) and then they were cut (c: cut) and the surface and the "bulk" was investigated [3].*

***FIGURE G2:** Si concentration smoothed over 10 single spectra (averaged over an area of 1x10 mm^2). The different line scans on each specimen are indicated by different fillings of the symbols.*

Appendix H: Some additional SEM images

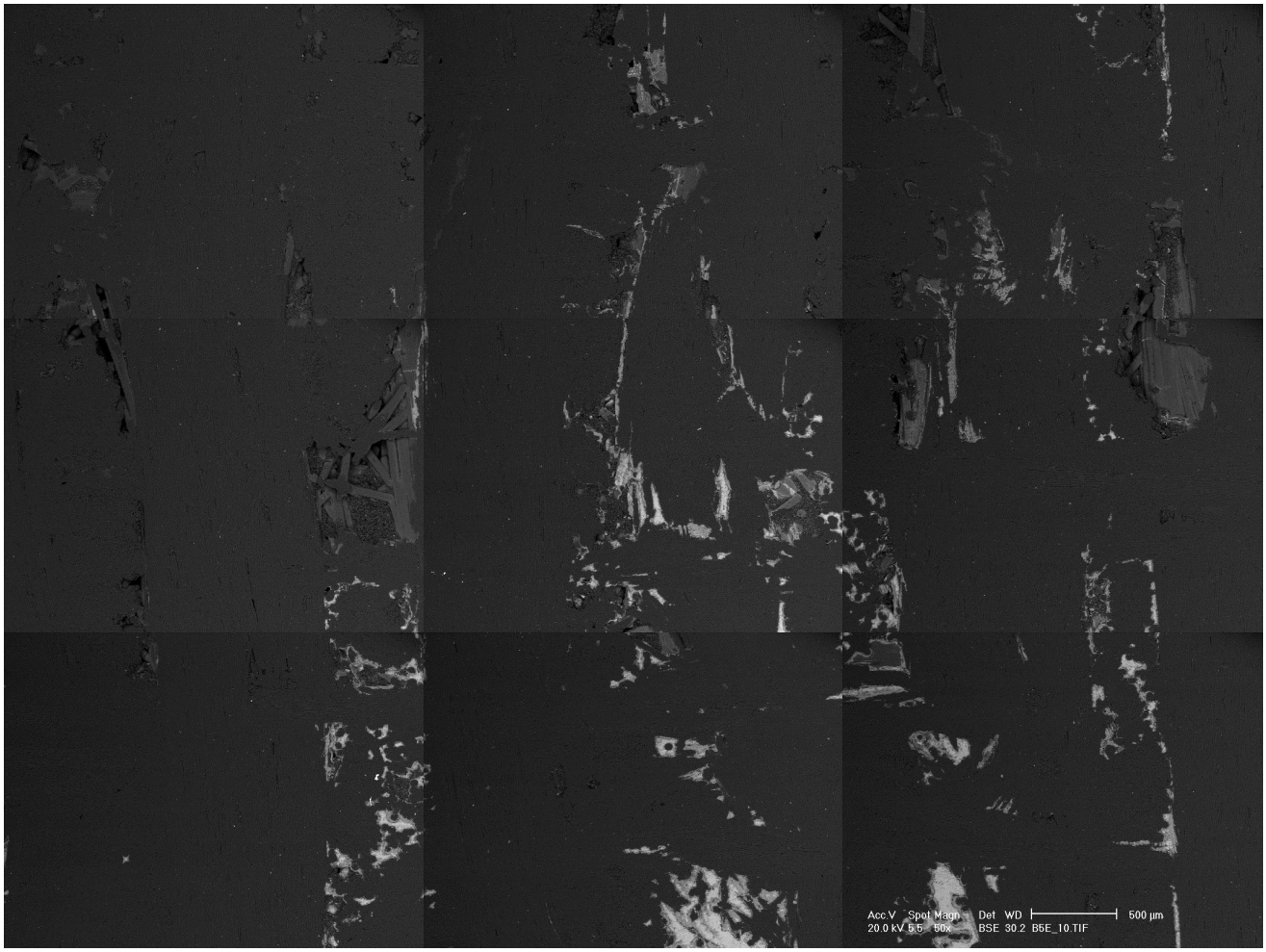

FIGURE H1*: Nine SEM images of backscattered electrons in low magnification of specimen* ***B5e*** *are merged together to cover an area of ~7.3×5.4 mm^2.*

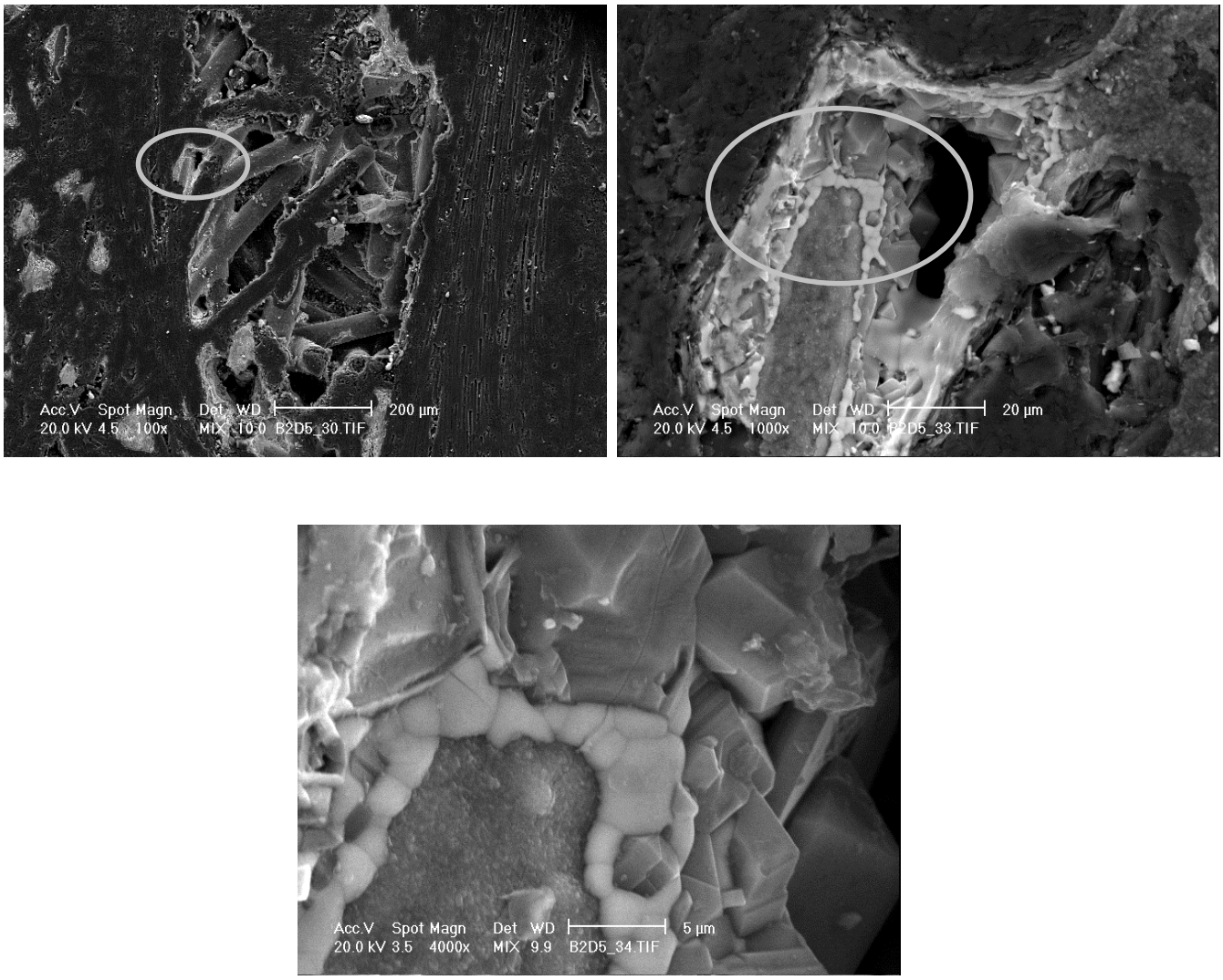

***FIGURE H2**: SEM images of a pore in the specimen **B2d #5** before heating test in different magnifications using a mixture of secondary and backscattered electrons. Fibres with Si/SiC cover are clearly visible. The worm-like structure in the centre and the crystal above the centre has been proven to consist of iron and SiC, respectively.*

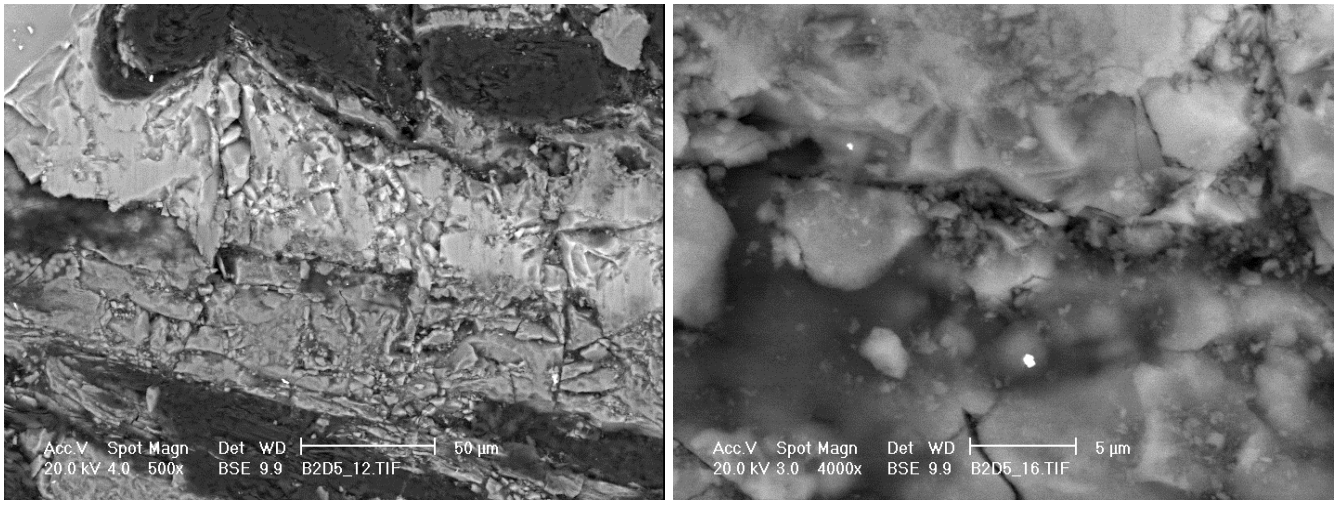

***FIGURE H3**: Blow up series of Si/SiC area on specimen **B2d #5** before the heating test. Small bright particle below centre of the right image has been proven to contain tungsten.*

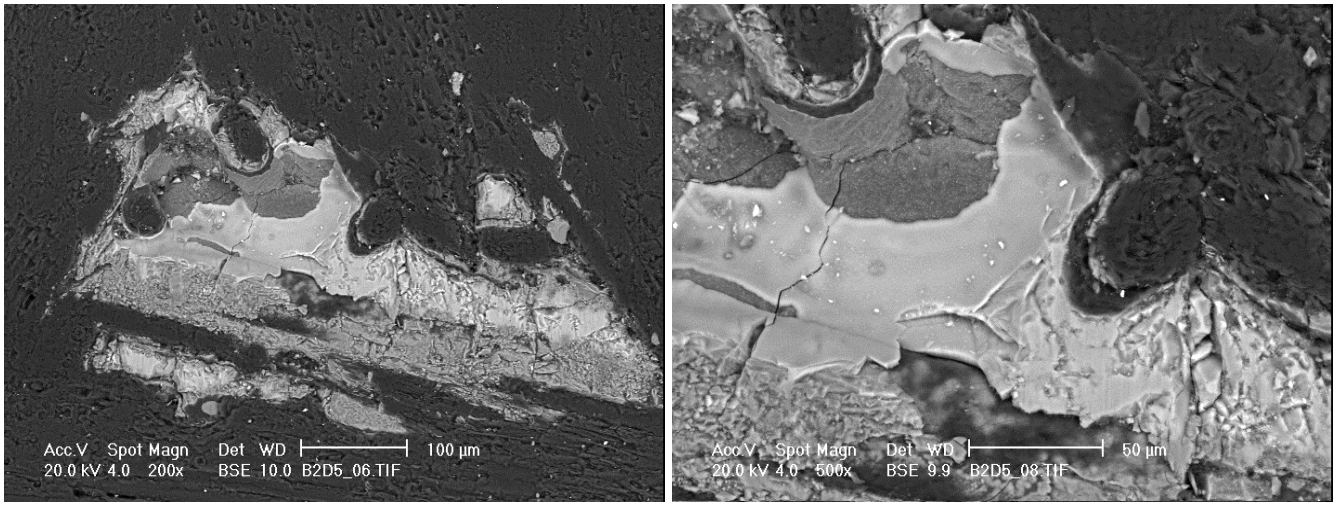

***FIGURE H4**: Blow up series of Si/SiC area on specimen **B2d #5** before the heating test.*

a)

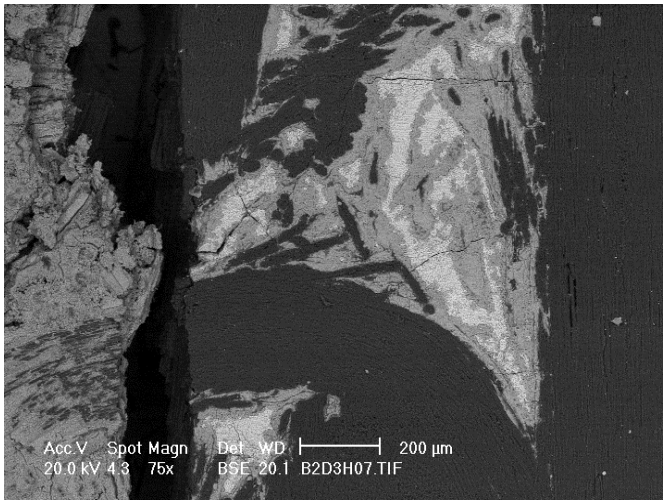

b)

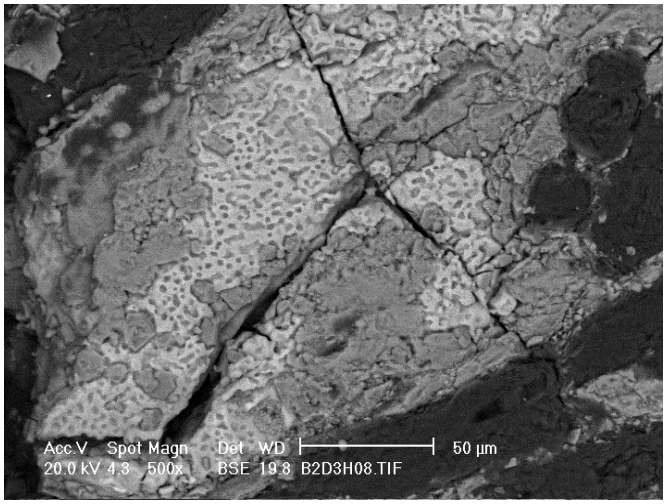

c)

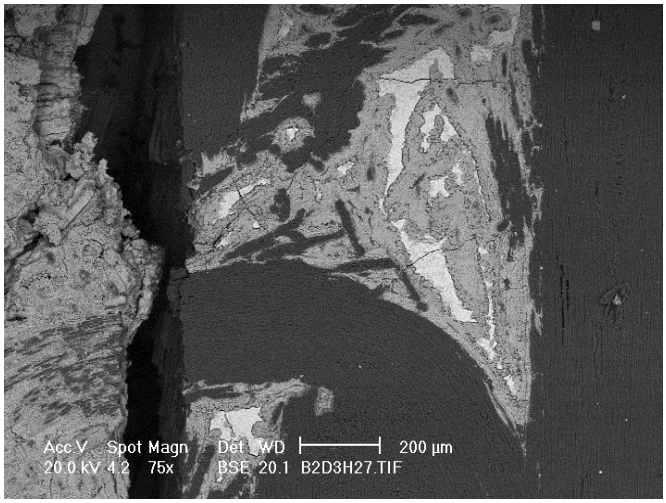

d)

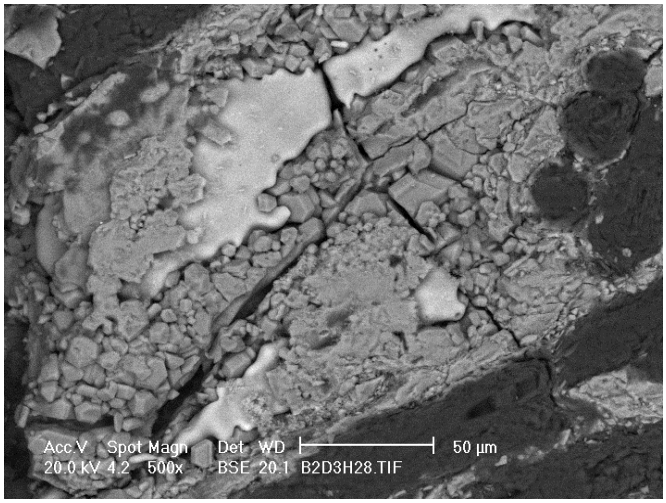

***FIGURE H5**: Blow up series of Si/SiC area on specimen **B2d #3** after heating for 10 minutes (a, b) and for 70 minutes at 1470 K (c, d). In a) and c) the specimens **B2d #4** after heating for 10 minutes at 1570 K is visible on the left side.*

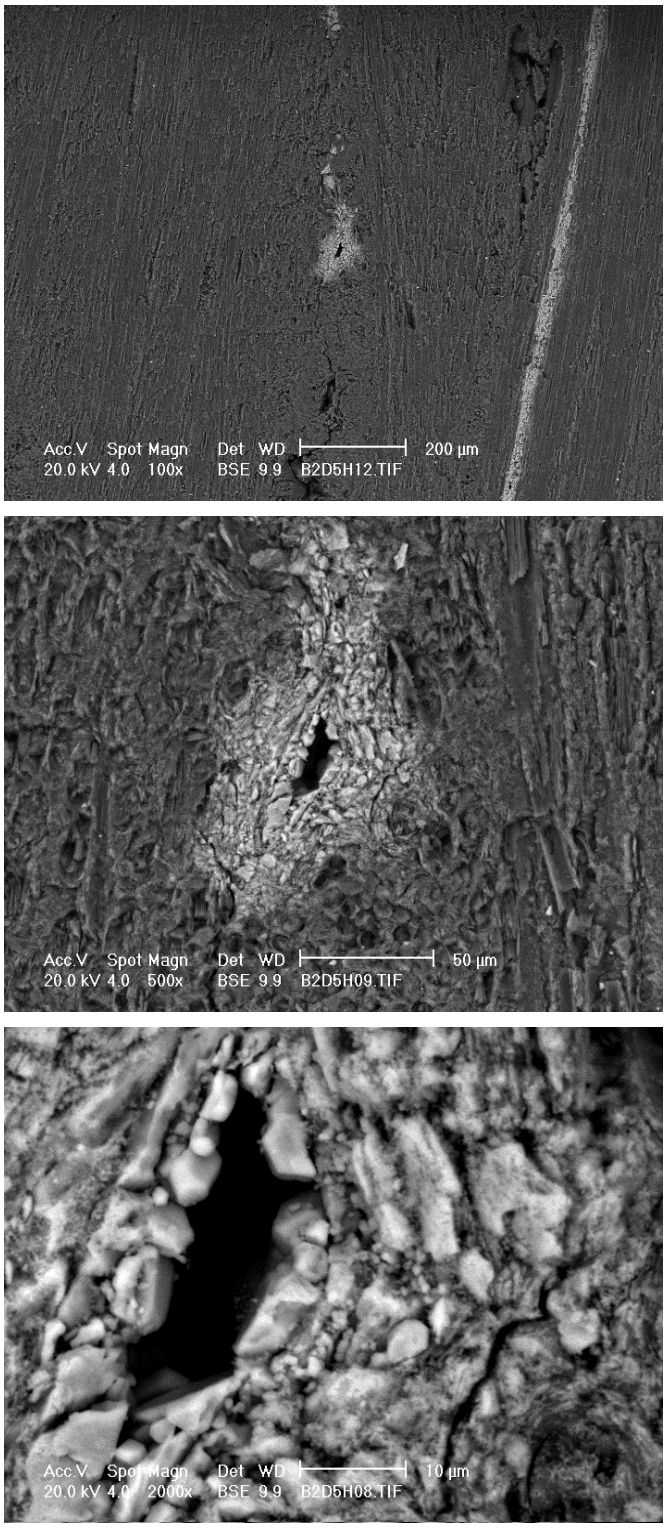

***FIGURE H6**: Blow up series of a pore on specimen **B2d #5** after heating for 10 minutes at 1700 K. The Si seem to be diffused out of the pore and formed SiC crystallites.*

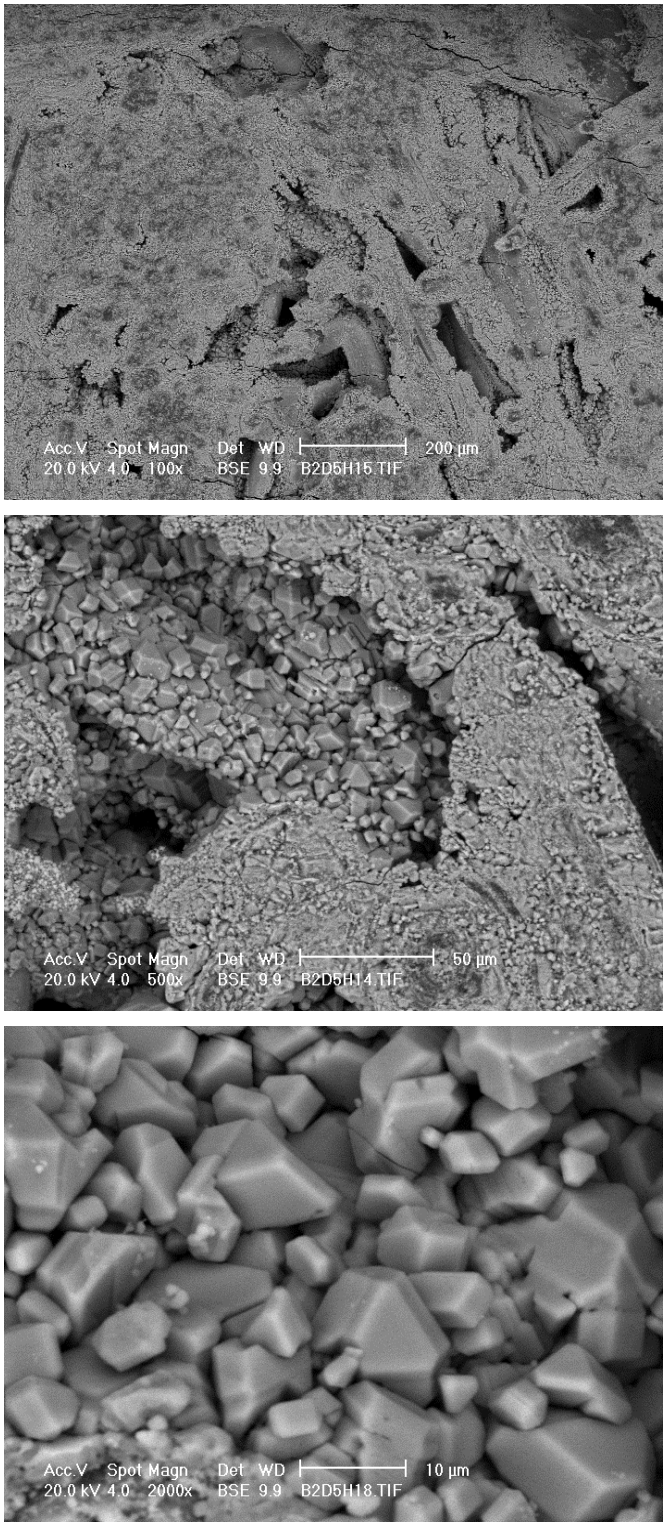

***FIGURE H7**: Blow up series of SiC area on specimen **B2d #5** after heating for 10 minutes at 1700 K. This region is totally covered with SiC crystallites.*

References

[1] M. Mayer, *SIMNRA User's Guide*, Tech. Rep. IPP9/113, Max-Planck-Institut für Plasmaphysik, Garching, (1997).

[2] JCPDS - International Centre for Diffraction Data (ICDD), PDF data base

[3] M. Balden, *Thermal stability and erosion of the silicon doped CFC material NS31*, Tech. Rep. IPP 9/112, Max-Planck-Institut für Plasmaphysik, Garching, (1997)

This final report will be published also as M. Balden, *Assessment of the Si content of Si impregnated Carbon-Carbon Fibre composite,* Tech. Rep. IPP 17/2, Max-Planck-Institut für Plasmaphysik, Garching, (2004)